Modeling and Simulation of a Prototypical Advanced Reactor

A Thesis Presented for the
Master of Science
Degree
The University of Tennessee, Knoxville

Xiaotong Liu
December 2015

Copyright © 2015 by Xiaotong Liu
All rights reserved.

Acknowledgements

The author would like to thank and acknowledge the advice, mentoring, and guidance provided by Dr. Jamie B. Coble, and also other members of the graduate committee Dr. J Wesley Hines and Dr. Belle R. Upadhyaya.

Abstract

Current online risk monitors provide a point-in-time estimate of the system risk given the current plant configuration (e.g., equipment availability, operational regime, environmental conditions). However, these risk monitors do not account for plant-specific normal, abnormal, and deteriorating states of active components and systems. The lack of operating experience with proposed advanced reactor designs limits our ability to estimate the probability of failure (POF) of key components. Incorporation of unit-specific estimates of POF into dynamic probabilistic risk assessment (PRA) has the potential to enable real-time decisions about stress relief and to support effective maintenance planning while ensuring investment protection. The enhanced risk monitor (ERM) supports the safe and economic operation goals of advanced reactor by providing a dynamic assessment of system risk with real-time estimates of POF and event probability based on equipment condition assessment. A simulation framework for a prototypical advanced reactor (PAR) was developed in this work to provide a platform to demonstrate the ERM.

A Simulink model of the PAR was developed, including the primary system, intermediate heat transport loop, steam generator, and balance of plant (BOP). To ensure accuracy across a large range of operating conditions, a nonlinear model for the primary system, including reactor kinetics and heat transfer, was used. A perturbation model of the steam generator showed good performance across the range of conditions and was thus employed. The PAR power block features two independent primary systems, each with dedicated intermediate heat exchangers and steam generators. These two modules are connected to a common BOP through a steam header. To balance the power output of each unit to meet overall power demand, fuzzy control is implemented in the primary system.

Degradation of the primary and intermediate sodium pumps is numerically simulated to investigate the effect on overall plant performance. The results indicate that the core power decreases as pump degradation leads to reduced flow in either primary or intermediate loops. The developed PAR model provides simulated power block performance data under component degradation, which can be used to develop and demonstrate the ERM framework.

Table of Contents

Chapter 1 Introduction 1
1.1 Research Objective 3
1.2 Thesis Organization 3

Chapter 2 Description of the Prototypical Advanced Reactor 4
2.1 Reactor Core and Intermediate Heat Exchanger 4
2.1.1 EBR-II 4
2.1.2 Functional Description of EBR-II 6
2.1.3 Reactor Core 6
2.1.4 IHX 6
2.2 Steam Generator 6
2.3 Steam Header 6
2.4 Balance of Plant 7
2.5 Multi-Modular Concepts 7
2.6 Probability Risk Assessment 8

Chapter 3 The Development of the Prototypical Advanced Reactor 10
3.1 The Development of the Primary System 10
3.1.1 Reactor Core Equations 10
3.1.2 Reflector and blanket models 13
3.1.3 Piping and plenum model 14
3.1.4 Intermediate Heat Transfer 15
3.1.5 Control Design 17
3.2 The Development of Once-Through Steam Generator 17
3.2.1 Evaporator and Drum Balance Equations 17
3.2.2 Superheater State Equations 22
3.2.3 Control Design 22
3.3 The Development of Balance of Plant 23

Chapter 4 Control Strategy and Model Validation 25
4.1 Steam Header 25
4.2 Feedback Between Units 27
4.3 Daily Load Profile 27
4.4 Steam Generator Control Design 28
4.5 Model Validation 28

Chapter 5 Pump Degradation Modeling and Response 34
5.1 Pump Degradation Modeling 34
5.2 Pump Degradation Response 35

Chapter 6 Summary and Future Work 43

List of References 44

Vita..... 46

List of Figures

Figure 1.1 Layout of pool-type SFR [2]…… 2
Figure 2.1 Prototypical advanced reactor power blocks [1]……... 5
Figure 3.1 Node representation of EBR-II primary system.…… 11
Figure 3.2 Mann's core heat transfer model [6]……..... 13
Figure 3.3 Lumped parameter approximation of a counterflow heat exchanger ……… 15
Figure 3.4 Nodal representation of EBR-II steam generator……..... 18
Figure 3.5 Balance of Plant Flow Diagram [12]……... 24
Figure 4.1 Schematic diagram of a multi-modular power block [5]…… 26
Figure 4.2 Power level for daily load profile…… 27
Figure 4.3 Perturbation model response of superheated steam temperature to a -5 cents reactivity perturbation……... 29
Figure 4.4 Perturbation model response of drum pressure to a -5 cents reactivity perturbation……... 30
Figure 4.5 Step response of fractional reactor power to a -5 cents reactivity perturbation in (lower) PAR model and (upper) EBR-II model [6]…….. 31
Figure 4.6 Step response of sodium tank temperature to -5 cents reactivity perturbation in (lower) PAR model and (upper) EBR-II model [6]…….. 32
Figure 4.7 Step response of fractional reactor power to different reactivity perturbation……... 33
Figure 5.1 Degraded pump curves [10]…… 34
Figure 5.2 Fractional power with different secondary side flow rate……... 35
Figure 5.3 Fractional power with different primary side flow rate……... 36
Figure 5.4 Core Fractional Power response to complete loss of flow in (upper) primary and (lower) secondary sodium…….. 37
Figure 5.5 Step response of fractional power with the degraded intermediate sodium flow rate……. 38
Figure 5.6 Step response of fractional power with the degraded primary sodium flow rate……. 39
Figure 5.7 Fractional power with degraded primary or intermediate sodium pump…… 40
Figure 5.8 Total power output with the primary pump degradation in module 1……. 41
Figure 5.9 Total power output with the intermediate pump degradation in module 2…. 42

Chapter 1

Introduction

The development of advanced reactors faces significant technique hurdles to commercialization due to the unique characteristics inherent to their designs, such as new component designs, harsh environments, and longer cycles between refueling outages. These features, along with the relative lack of operating experience with advanced coolants and component designs, will challenge our ability to accurately characterize the evolving risk of operating advanced reactors. Current online risk monitors provide a point-in-time estimate of the system risk given the current plant configuration (e.g., equipment availability, operational regime, environmental conditions). However, these risk monitors do not account for plant-specific normal, abnormal, and deteriorating states of active components and systems. Incorporation of unit-specific estimates of the probability of failure (POF) of key components into dynamic probabilistic risk assessment (PRA) has the potential to enable real-time decisions about stress relief and to support effective maintenance planning while ensuring investment protection. Such enhanced risk monitors (ERMs) are expected to improve the safety, economy, and availability of advanced reactors [1].

The ERM can support the safety and economic goals of advanced reactors by optimizing operations and maintenance activities. Asset management and optimization are important to ensure the safety and optimize the economics of advanced reactors. Advanced plant configuration, condition, and risk monitors are needed to support frequently changing plant configurations. The optimization of assets through ERMs will improve economics of advanced reactors by maximizing generation, supporting reduced operations and maintenance staff, and improving plant and equipment availability.

To support the development and demonstration of the ERM framework, a prototypical advanced reactor (PAR) design was modeled in MATLAB-Simulink. The PAR power block includes two independent reactor cores, each connected to a dedicated intermediate heat exchanger and steam generator. Steam from the two modules is mixed in a steam header and sent to a common balance of plant. The PAR design is based on a sodium fast reactor (SFR), though the ERM is more generally applicable to any advanced or light water reactor design. The Generation IV Technology Roadmap identifies the SFR as a promising technology to perform in particular the missions of sustainability, actinide management, and electricity production if enhanced economics for the system could be realized [18]. The primary coolant system can either be arranged in a pool layout where all primary system components are housed in a single vessel, or in a compact loop layout. Most current SFR designs favor a pool-type primary system to avoid concerns of large break loss of coolant accidents. A typical layout of pool-type SFRs is shown in Figure 1.1.

The PAR model explicitly models the major reactor systems and numerically simulates the degradation of key active components. The effect of component degradation on the overall power production of the PAR is simulated to support demonstration of the ERM.

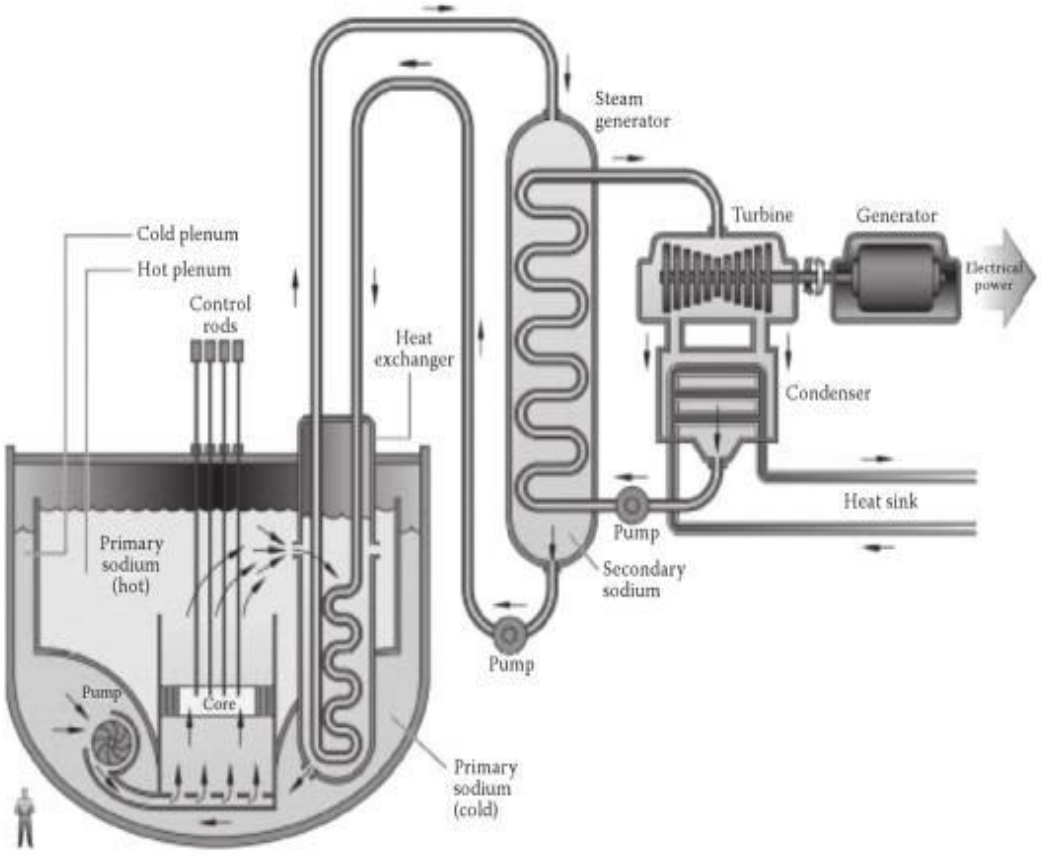


Figure 1.1 Layout of pool-type SFR [2]

This report summarizes the development of the PAR, including simulation of major components and systems, reactor control schemes, and component degradation models. Initial simulation results are presented for degradation of sodium pumps in the primary and intermediate loops.

1.1 Research Objective

The development and deployment of advanced reactor face significant technique hurdles to commercialization due to their unique operational characteristics and relative lack of operational experience. The enhanced risk monitor is being developed as one approach to compensate for this lack of operational data, by providing an accurate and dynamic assessment of the safety and economic risks of operating. In order to demonstrate the efficacy of the ERM for advanced reactors, a Simulink-based model of the PAR design has been developed at the University of Tennessee (UT). The PAR simulation platform can be used to simulate the effects of primary and intermediate sodium pump degradation and is extensible to other component degradation models. This simulation model can be used to generate data to test and demonstrate the ERM under degraded component operation.

1.2 Thesis Organization

An overview of the prototypical advanced reactor is provided in Chapter 2. This includes a general description of the major components, such as the reactor core, intermediate heat exchanger, steam generator, steam header and balance of plant.

Chapter 3 presents the models of key subsystems, including the primary reactor system, steam generator, and balance of plant. The primary system and intermediate heat exchanger model is based on Berkan and Upadhyaya [6]. This model includes point reactor kinetics and Mann's heat transfer model, of which the nodalization and assumptions are discussed. The primary system includes the reactor kinetics, core heat transfer, reflector and blanket, piping and plenum, intermediate heat exchanger, and primary system control strategy. Model validation results for the primary system are compared with reference [6]. This discussion is followed by a description of the once-through steam generator model [6], which includes the evaporator, steam drum, and superheater. The major steam generator control system, the steam pressure controller, is described. Finally, the development and adaption of the balance of plant (BOP) [13] is presented. The method for resizing the BOP model to meet the total PAR output is described.

The use of multi-modular control strategies is discussed in Chapter 4. This includes the strategy used to develop steam header and feedback between units. In addition, the method to arrange the power level for each module to meet the daily load is discussed.

Simulations of the model and degradation of primary and intermediate sodium pumps are discussed in Chapter 5.

Finally, concluding remarks, recommendations, and future work are discussed in Chapter 6.

Chapter 2

Description of the Prototypical Advanced Reactor

Work on the ERM has focused on liquid metal reactors to demonstrate the efficacy of the approach, although the framework is generally applicable to any advanced reactor; light water reactor; and other high-value, mission critical non-nuclear systems. The working prototypical advanced reactor (PAR) design is shown in Figure 2.1. This power block features two reactor cores, each connected to a dedicated intermediate heat exchanger (IHX) and steam generator. The output of these two steam generators is then connected to a common balance of plant (BOP). BOP includes steam drums, turbine, condenser, feedwater pumps, and feedwater heaters. The key components identified in this power block that require physical models include: reactor core, IHX, steam generator, and BOP. Additional components that play in to the ERM demonstration include pumps, valves, reactor vessel auxiliary cooling system (RVACS), and steam generator auxiliary cooling system (ACS). The effects of evolving degradation and failure of key components on the overall system performance can be modeled.

The three primary systems in the PAR: reactor core and IHX, steam generator, and BOP, are briefly described in the following sections, followed by a discussion of considerations for multi-modular plants and the simplified probabilistic risk assessment for the PAR. The models for these systems are described in detail in Chapter 3.

2.1 Reactor Core and Intermediate Heat Exchanger

The reactor core and IHX are modeled based on the Experimental Breeder Reactor EBR-II. EBR-II was a pool-type sodium-cooled fast reactor (SFR). EBR-II featured 62.5 MWt with 20 MWe output. The prototypical advanced reactor features two EBR-II cores connected to a common BOP, giving a total of 40 MWe output for the power block. Existing perturbation models of EBR-II core and IHX provide a starting point for modeling [6]. These perturbation models are linearized at 100% nominal power. Nonlinear equations are derived from these models in order to support simulations of normal transient operation across a wide range of power demand.

2.1.1 EBR-II

The Experimental Breeder Reactor was a liquid metal fast breeder reactor. The plant primarily consists of three loops: primary loop, which contains the sodium-cooled reactor; an intermediate sodium coolant loop and the secondary loop, which is the steam generator. This concept is also referred to as the pool-type design because the reactor, primary coolant system and the fuel-handling system components are submerged in a large primary sodium tank.

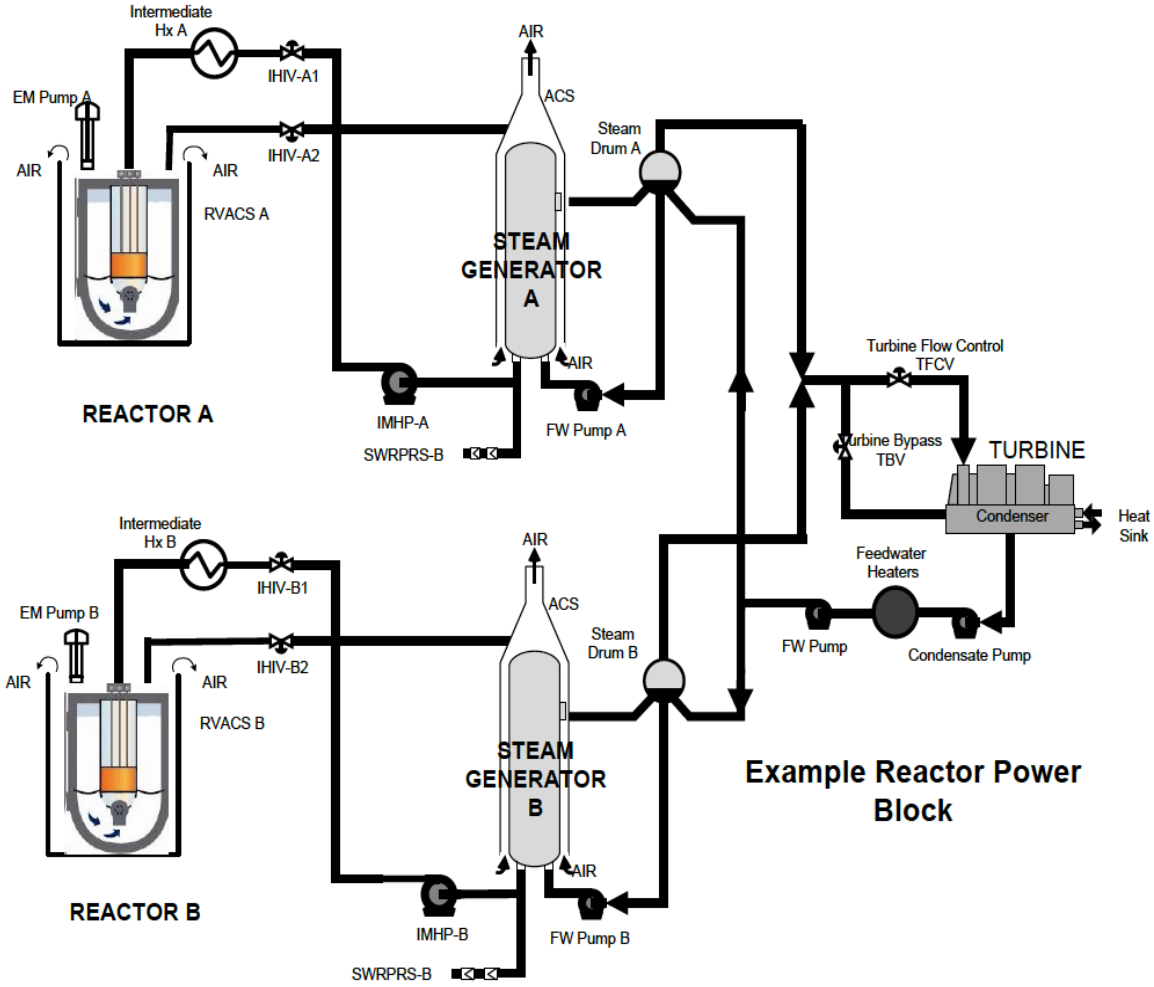


Figure 2.1 Prototypical advanced reactor power blocks [1]

2.1.2 Functional Description of EBR-II

The reactor generates the heat by nuclear fission, which is absorbed by liquid sodium that circulates the primary loop. The absorbed heat is transferred to secondary loop by an intermediate heat exchanger so that there is no radioactive sodium in steam generator. The heat is used to generate superheated steam that drives a turbine generator to produce electricity. The steam is condensed to water, then pumped back into the steam generator as cooling water.

2.1.3 Reactor Core

The core consists of upper blanket, active core, and lower blanket. The upper and lower blanket subassemblies consists of 19 pins each, and each 18 inches long. The reactor core consists of 53 fuel subassemblies, 12 control rod subassemblies and 2 safety rod assemblies. Each fuel assembly consists of 91 fuel elements. Each fuel assembly consists of 91 fuel elements. The equivalent active core diameter is 19.94 inches and has a height of 14.22 inches

2.1.4 IHX

IHX is fixed above the reactor vessel. The primary coolant enters the shell side of IHX, flows down and discharges into the primary tank. The intermediate sodium enters and leaves the IHX at the top, flowing through tubes in the IHX.

2.2 Steam Generator

The steam generator produces superheated steam at 820F, 1250 psig using the heat delivered by the intermediate loop. The steam generator consists of a steam drum, two once-through super-heaters and seven shell-and-tube recirculating evaporators. Each reactor core/IHX model will be connected to a dedicated steam generator.

The feedwater absorbs heat from the sodium on the shell side, and is returned to the steam drum. The saturated steam-water mixture reaches the superheater to become superheated steam. Then, the moisture separating components can separate the dry steam from water from saturated steam-water mixture.

2.3 Steam Header

The multi-modular reactor system consists of two integral EBR-II reactors. Each unit has a power of 20 MWe and operates in parallel, with the steam from the two units flowing into a steam header. Such power generating stations have the advantages of providing continuous power supply when one of the units is down for maintenance and load following features with the units operating at different power levels [5].

2.4 Balance of Plant

Finally, the steam header is connected to a common balance of plant (BOP). The BOP system components include the following:

- Turbine-generator system;
- Condenser;
- Condensate pump, secondary feedwater pumps, and main feedwater pump;
- Multiple feedwater heaters.

An existing BOP model [13] is leveraged here. The BOP model was originally designed for a 180 MWe SMR, key components were resized to match total power output available in the PAR.

2.5 Multi-Modular Concepts

Issues in the control of multi-modular reactor plants are discussed with emphasis on the need for operation under conditions of unbalanced loads, operation strategies for both single and multi-reactor systems, and the coordinated adjustment of power and temperature [3].

One defining characteristics of a multi-modular plant is that each unit will probably be loaded differently so as to compensate for the effects of varying maintenance outages and, if desired, to stagger refueling; A second characteristic is interdependency in that, with several reactors connected to a common turbine, a change in any one unit will propagate to the others. The combination of these two factors makes operation of a multi-modular plant differ from that of existing single-reactor ones. For example, conventional sliding-T_{avg} load maps cannot be applied directly to a multi-modular system because, with the exception of the highest-powered unit, each reactor's temperature will be a function of not only its power level but also that of the most heavily loaded one [4].

Similarly, withdrawal of the control rods in a fully loaded PWR will, in the presence of a large negative temperature coefficient, cause hot and cold leg temperatures to rise but leave power and core ΔT unchanged. In a multi-modular system, there will be a shift in power to the affected reactor. These and other differenced in the behavior of multi-modular and single-reactor systems are delineated.

Specific advantages to the multi-modular approach are as follows [5].

- The small size of the reactor core may allow the incorporation of passive safety features such as natural circulation cooling on loss of off-size electricity.

- The individual modules are to be sized so that components related to nuclear safety can be factory-fabricated. This will allow quality to be more readily controlled.

- Once the major components are made, they are to be transported to the site for rapid installation. This construction method is expected to reduce the licensing effort because the modules will be pre-licensed, and only site-specific issues will have to be considered in the final licensing process.

- The small size of the components and the simplicity of the power loop should reduce maintenance.

- Multi-modular power plants have the potential to provide higher capacity factors than do large, single-reactor plants because the modular makeup will ensure partial power output from unaffected units whenever any one module is off-line for refueling or maintenance.

One means of operating a multi-modular plant would be to distribute the load equally. Thus, all reactors would operate at the same temperature and pressure and, from the perspective of plant control, the modules would respond as if they were a single, large reactor.

2.6 Probability Risk Assessment

Probabilistic Risk Assessment (PRA) has emerged as an increasingly popular analysis tool during the last decade. PRA is a systematic and comprehensive methodology to evaluate risks in complex engineering systems. In general, risk can be defined as the product of the frequency and its consequence. Online risk monitors and the proposed ERM are built on the system PAR model.

The initial PRA model for the PAR includes the following components [1]:

- Sodium pumps
- RVACS
- Emergency diesel
- Steam generator (tube rupture)
- Liquid metal sodium pressure relief system
- Isolation valve
- Feedwater pump
- Steam generator louvers
- Intermediate sodium pump
- Condensate pump
- IHX tube rupture
- Turbine bypass valve

In the nuclear industry, events that have consequences related to public safety are evaluated for risk. The evaluation process for the risk with respect to nuclear power plants involve identifying initiating events and event sequences, providing realistic quantitative measures of the likelihood of the risk contributors, a realistic evaluation of

the potential consequences, and a framework for making decisions. Risk monitors incorporate the actual plant configuration into the risk assessment so that the PRA framework can be extended. The ERM incorporates equipment condition into the probability of component failure for a more accurate estimation of operational risk.

And the following chapters present the equations and models for key PAR subsystems, including primary system, steam generator, balance of plant, and multi-modular control system.

Chapter 3

The Development of the Prototypical Advanced Reactor

3.1 The Development of the Primary System

The primary system consists of reactor, primary cooling systems, neutron shield, fuel handling system, control and safety drive systems, tank and biological shield, fuel unloading and inter-building transfer, primary sodium purification system and argon blanket gas system. For the purpose of the PAR model, only the reactor and primary cooling system are modeled.

A node formulation of the primary loop and the intermediate heat exchanger is presented in Figure 3.1. The primary loop includes the active core, inner and outer blankets, lower and upper reflectors, and piping. The formulation of the whole model and all the parameters are adapted using the models in [6].

The intermediate heat exchanger consists of 10 nodes. The primary loop and IHX models are coupled into one module for the convenience of simulation studies. The governing equations for each subsystem and the definition of variables are presented in the following sections. Parameter value for each constant can be found in [6].

Node 1 is the fractional reaction power, and node 2 is the precursor concentration. Nodes 3 through 37 are the temperature in appropriate regions of the primary system. Nodes 3 through 7 are the active cores. Node 8, 9 and 10, 11 are the low and high. Nodes 12 through 14 are the lower reflector. Nodes 15 through 17 are the upper reflector. Nodes 18 through 20 are the inner blankets. Nodes 21 through 23 are the outer blankets. Node 24 is the upper plenum. Nodes 25 and 26 are the IHX inlet plenum. Nodes 27 through 36 are the IHX. Node 37 is the sodium tank

3.1.1 Reactor Core Equations

The reactor contains the fuel material and blanket material, which are all in the reactor vessel. In addition to the fuel material, fuel bearing subassemblies consists of upper and lower axial blanket regions. The active core dynamics are described by the point reactor kinetics equations

1) Nonlinear reactor kinetics

$$\dot{P}_c = -\frac{\beta_T}{\Lambda} P_c + \frac{\rho P_c}{\Lambda} + \bar{\lambda} C \tag{3.1}$$

$$\rho = \rho_{external} + \rho_{feedback}$$

$$\rho_{feedback} = \sum_i \alpha_i (T_i - T_{io})$$

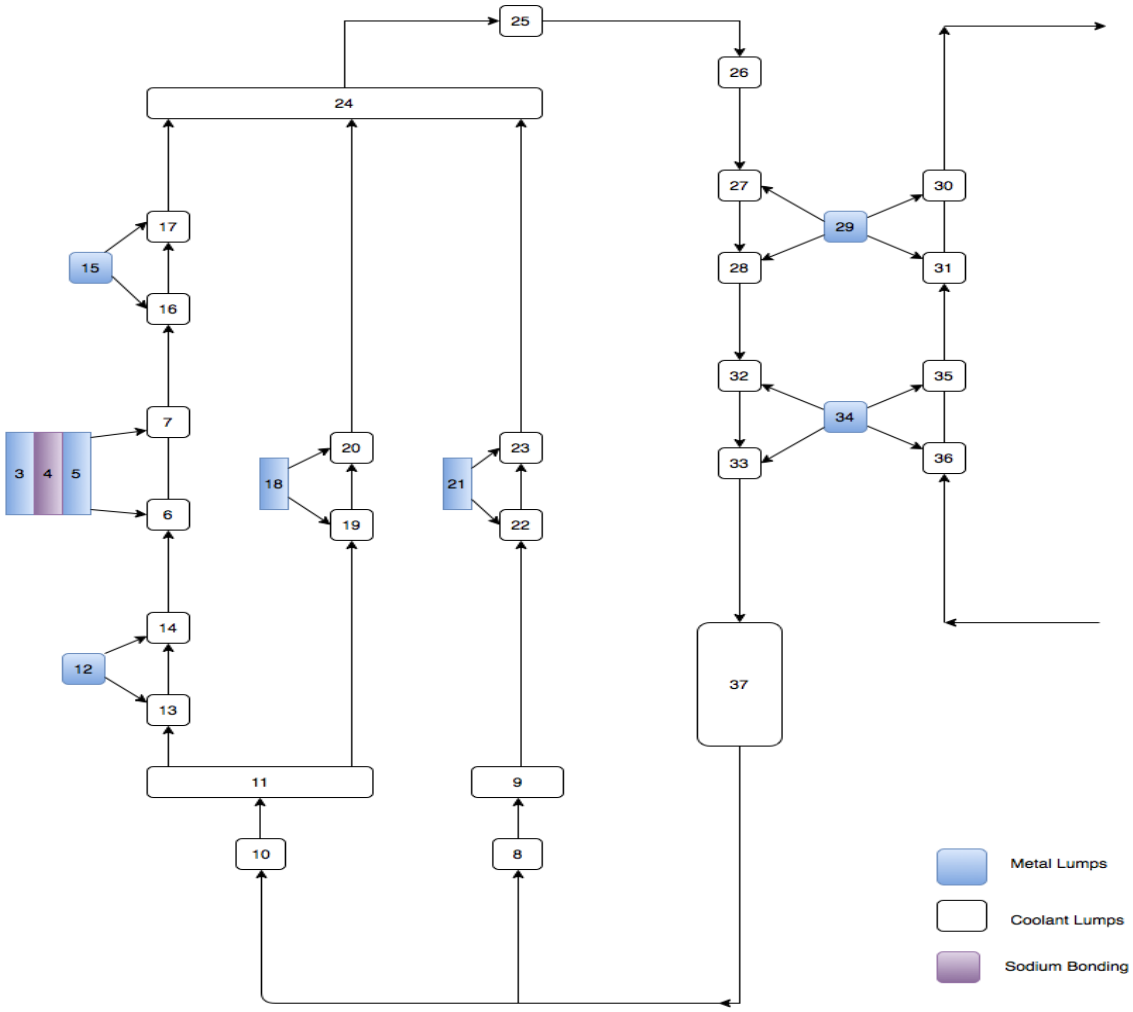


Figure 3.1 Node representation of EBR-II primary system

$$\dot{C}_c = \frac{\beta_T}{\Lambda} P_c - \bar{\lambda} C_c \quad (3.2)$$

$$C = C_c + C_o$$

$$C_o = \frac{\beta_T P_{co}}{\Lambda \bar{\lambda}}$$

where:
P_c = Fractional Core Power
β_T = Total Delay Neutron Fraction
Λ = Mean Neutron Generation Time
ρ = Reactivity
$\bar{\lambda}$ = Precursor Average Decay Constant
C = Precursor Concentration
α_i = Temperature Reactivity Feedback Corresponding to Temperature T_i
T_i = Current Temperature in Channel i
T_{io} = Steady State Temperature for Channel i at 100% power.

2) Core heat transfer

Five differential equations correspond with the five lumps are shown in Figure 3.2. Mann's model is used to represent the heat transfer dynamics. Average lump temperature is a coupling parameter for the driving force of heat transfer between the coolant and metal nodes. The lower coolant lump outlet temperature is assumed to present the average lump temperature in Mann's model.

$$\dot{T}_F = \frac{P_f P_o}{(MC_p)_F} P_c - \frac{1}{R_1 (MC_p)_F} (T_F - T_B) \quad (3.3)$$

$$\dot{T}_B = \frac{1}{R_1 (MC_p)_B} (T_F - T_B) - \frac{1}{R_2 (MC_p)_B} (T_B - T_C) \quad (3.4)$$

$$\dot{T}_C = \frac{1}{R_2 (MC_p)_B} (T_B - T_C) - \frac{1}{R_3 (MC_p)_\theta} (T_B - \theta_1) \quad (3.5)$$

$$\dot{\theta}_1 = \frac{1}{R_2 (MC_p)_\theta} (T_C - \theta_1) + \frac{2}{\tau} (\gamma_2 - \theta_1) \quad (3.6)$$

$$\dot{\theta}_2 = \frac{1}{R_3 (MC_p)_\theta} (T_C - \theta_1) + \frac{2}{\tau} (\theta_1 - \theta_2) \quad (3.7)$$

where:
T_F = fuel temperature
T_B = sodium-bond temperature
T_C = fuel cladding temperature

θ_i = temperature of the ith coolant node
R_1, R_2, R_3 = heat transfer resistances,
γ_2 = lower axial-reflector coolant outlet temperature
τ = resident time of the coolant in the active core region
P_F = fraction of the power deposited in the fuel
$(C_p)_F$ = specific heat capacity of the fuel
$(C_p)_B$ = specific heat capacity of the blanket material
$(C_p)_\theta$ = specific heat capacity of the coolant
M_F = mass of the fuel
M_B = mass of the blanket material
M_θ = mass of the coolant

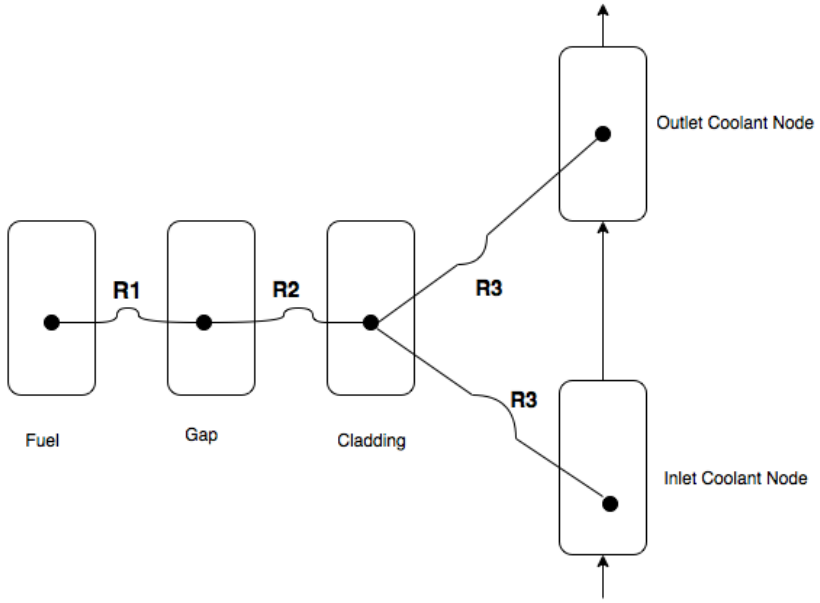


Figure 3.2 Mann's core heat transfer model [6]

3.1.2 Reflector and blanket models

In the EBR-II, reflectors and blankets surround the reactor core. The core model consists of twelve nodes representing the reflector and radial blanket region. The same heat transfer principle used in the core heat transfer model is also applied to develop the state equations. The equations for every reflector and blanket regions are described each by a set of three equations as shown below.

$$\dot{T}_M = \frac{P_i}{(MC_p)_M} P_c - \frac{U*A}{(MC_p)_M} \quad (T_M - T_1) \tag{3.10}$$

$$\dot{T}_1 = \frac{U*A}{(MC_p)_T} \quad (\delta T_M - \delta T_1) + \frac{2}{\tau}(\theta_{in} - T_1) \tag{3.11}$$

$$\dot{T}_2 = \frac{U*A}{(MC_p)_T} \quad (\delta T_M - \delta T_1) + \frac{2}{\tau}(T_1 - T_2) \tag{3.12}$$

where:
T_M = temperature of the metal node
T_1 = temperature of the first region coolant node
T_2 = temperature of the second region coolant node
A = total heat transfer area
τ = residence time of the coolant in the reflector or the blanket region
U = metal to coolant heat transfer coefficient
θ_{in} = inlet coolant temperature
$(C_p)_M$ = specific heat capacity of the metal
$(C_p)_T$ = specific heat capacity of the coolant

3.1.3 Piping and plenum model

The model consists of six nodes for the low and high pressure plenum, the upper plenum and core inlet-outlet piping region. A transfer-lag has been assumed for the piping. The other assumptions include: constant coolant density; no heat gain or loss in the piping; no axial heat conduction. The state equations are shown below.

$$\dot{T_U} = \frac{M_1 C_{p_2}}{(MC_p)_u}\gamma_4 + \frac{M_2 C_{p_2}}{(MC_p)_u}\gamma_6 + \frac{M_3 C_{p_3}}{(MC_p)_u}\gamma_8 - \left[\frac{M_1 C_{p_2}}{(MC_p)_u} + \frac{M_2 C_{p_2}}{(MC_p)_u} + \frac{M_3 C_{p_3}}{(MC_p)_u}\right] T_U \tag{3.8}$$

$$\dot{T_{out}} = \frac{1}{\tau_1} T_U - \frac{1}{\tau_1} T_{out} \tag{3.9}$$

$$\dot{T_{LI}} = \frac{1}{\tau_3}\theta_p - \frac{1}{\tau_3} T_{LI} \tag{3.10}$$

$$\dot{T_{HI}} = \frac{1}{\tau_4}\theta_p - \frac{1}{\tau_4} T_{HI} \tag{3.11}$$

$$\dot{T_H} = \frac{1}{\tau_5} T_{HI} - \frac{1}{\tau_5} T_H \tag{3.12}$$

$$\dot{T_L} = \frac{1}{\tau_6} T_{LI} - \frac{1}{\tau_6} T_L \tag{3.13}$$

where:
T_U = upper plenum temperature
T_{out} = reactor outlet temperature
θ_p = primary sodium tank temperature
T_{LI} = low-pressure plenum inlet temperature
T_{HI} = high-pressure plenum inlet temperature
T_H = high-pressure plenum temperature
γ_4 = upper reflector outlet temperature
γ_6 = inner reflector outlet temperature

γ_8 = blanket region outlet temperature
T_L = low-pressure plenum temperature
τ_1 = resident time of sodium in reactor outlet piping
τ_2 = resident time of sodium in the pot
τ_3 = resident time of sodium in the pot-to-reactor low-pressure piping
τ_4 = resident time of sodium in the pot-to-reactor high-pressure piping
τ_5 = resident time of sodium in the high-pressure plenum
τ_6 = resident time of sodium in the low-pressure

3.1.4 Intermediate Heat Transfer

Twelve nodes are used to represent the IHX and sodium tank as shown in Figure 3.3. The sodium tank and primary inlet plenum are represented by transport-lag approximations. Mann's model is also used for the heat transfer between the primary and intermediate loop sodium.

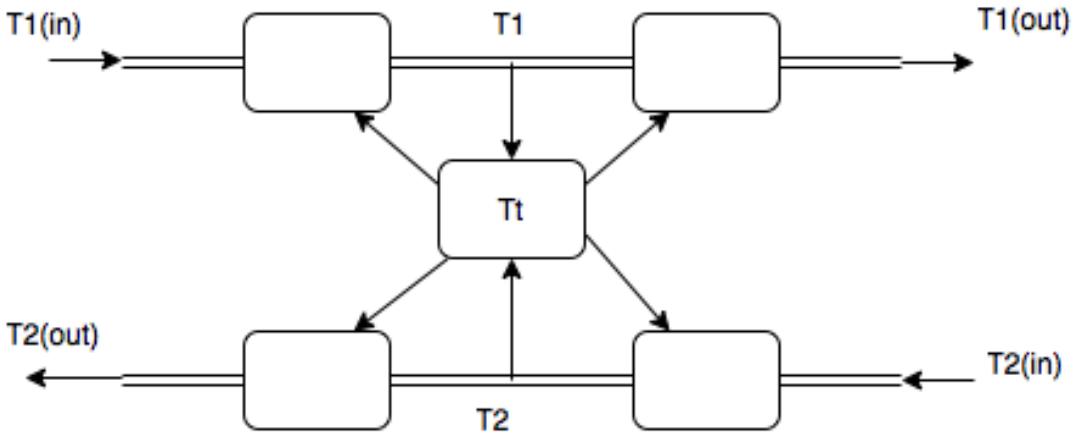


Figure 3.3 Lumped parameter approximation of a counterflow heat exchanger

$$\dot{P}_1 = \frac{2}{\tau_{HXP}} T_{HP} - \left(\frac{(UA)_P}{(MC_p)_P} + \frac{2}{\tau_{HXP}}\right) P_1 + \frac{(UA)_P}{(MC_p)_P} M_1 \tag{3.14}$$

$$\dot{P}_2 = \left(\frac{2}{\tau_{HXP}} - \frac{(UA)_P}{(MC_p)_P}\right) P_1 - \frac{2}{\tau_{HXP}} P_2 + \frac{(UA)_P}{(MC_p)_P} M_1 \tag{3.15}$$

$$\dot{M}_1 = \frac{(UA)_P}{(MC_p)_M} P_1 - \left(\frac{(UA)_P + (UA)_S}{(MC_p)_M}\right) M_1 + \frac{(UA)_S}{(MC_p)_M} S_3 \tag{3.16}$$

$$\dot{S}_4 = \frac{(UA)_S}{(MC_p)_S} M_1 - \left(\frac{(UA)_S}{(MC_p)_S} - \frac{2}{\tau_{HXS}}\right) S_3 - \frac{2}{\tau_{HXS}} S_4 \tag{3.17}$$

$$\dot{S}_3 = \frac{(UA)_S}{(MC_p)_S} M_1 - \left(\frac{(UA)_S}{(MC_p)_S} + \frac{2}{\tau_{HXS}}\right) S_3 + \frac{2}{\tau_{HXS}} S_2 \quad (3.18)$$

$$\dot{P}_3 = \frac{2}{\tau_{HXP}} P_2 - \left(\frac{(UA)_P}{(MC_p)_P} + \frac{2}{\tau_{XHP}}\right) P_3 + \frac{(UA)_P}{(MC_p)_P} M_2 \quad (3.19)$$

$$\dot{P}_4 = \left(\frac{2}{\tau_{HXP}} - \frac{(UA)_P}{(MC_p)_P}\right) P_3 - \frac{2}{\tau_{XHP}} P_4 + \frac{(UA)_P}{(MC_p)_P} M_2 \quad (3.20)$$

$$\dot{M}_2 = \frac{(UA)_P}{(MC_p)_M} P_3 - \left(\frac{(UA)_P + (UA)_S}{(MC_p)_M}\right) M_2 + \frac{(UA)_S}{(MC_p)_M} S_1 \quad (3.21)$$

$$\dot{S}_2 = \frac{(UA)_S}{(MC_p)_S} M_2 - \left(\frac{(UA)_S}{(MC_p)_S} - \frac{2}{\tau_{XHS}}\right) S_1 - \frac{2}{\tau_{XHS}} S_2 \quad (3.22)$$

$$\dot{S}_1 = \frac{(UA)_S}{(MC_p)_S} M_2 - \left(\frac{(UA)_S}{(MC_p)_S} + \frac{2}{\tau_{HXS}}\right) S_1 + \frac{2}{\tau_{HXS}} S_{in} \quad (3.23)$$

$$\dot{P_{in}} = \frac{1}{\tau_7} T_{out} - \frac{1}{\tau_7} P_{in} \quad (3.24)$$

$$\dot{\theta}_P = \frac{1}{\tau_2} P_4 - \frac{1}{\tau_2} \theta_P \quad (3.25)$$

where:
P_1 = first primary node temperature
P_2 = second primary node temperature
M_1 = first (upper) tube wall temperature
S_4 = fourth secondary node temperature
S_3 = third secondary node temperature
P_3 = third primary node temperature
P_4 = fourth primary node temperature
M_2 = second (lower) tube wall temperature
S_2 = second secondary node temperature
S_1 = first secondary node temperature
P_{in} = primary inlet plenum temperature
T_{out} = reactor outlet temperature
S_{in} = secondary sodium inlet temperature
θ_p = sodium tank temperature
τ_{HXP} = resident time in primary nodes
τ_{HXS} = resident time in secondary nodes
τ_7 = resident time in primary outlet plenum

3.1.5 Control Design

The external reactivity is used to simulate the function of control rad. And the two units work together to achieve the designed power level. In addition, the sodium pump in either the primary or intermediate loop may degrade failure conditions. A fuzzy control design is used to balance the external reactivity put in each unit to accommodate with the degraded flow rates so that the model can output a designed power level.

3.2 The Development of Once-Through Steam Generator

EBR-II steam generator is a once through natural circulation system. The steam generator is represented by twenty differential equations using the state-space technique. The nodal representation of the thirteen lumps representing average physical quantities is shown in Figure 3.4.

The single-phase heat transfer assumption is used in the superheater model. In addition, primary sodium flow is also assumed to be constant. The five state variables of the superheater model include the superheated steam, temperatures of the primary sodium and the tube wall. The other two state variables are the flow of feedwater and its control input.

3.2.1 Evaporator and Drum Balance Equations

On the evaporator side, the primary tube wall and the secondary lumps are divided with a moving boundary determined by the subcooled height [11]. Thermodynamic properties of the model are determined at drum pressure and pressure inside the tubes. The functions of these two pressures represent the system dynamics. The primary assumptions used in this model are: phase equilibrium; no superheating in the boiling region; the separators being 100% effective; the linear dependence between flow and enthalpy increase caused by the heat transfer into this region.

The evaporator side consists of thirteen state variables including the downcomer and drum water temperature, drum and boiling region pressures, drum inlet steam quality, subcooled level and drum level, primary sodium and tube wall temperatures, and two flows for the downcomer and rising mixture in the boiling region.

a Steam Drum

The equations for the steam drum are shown below.

$$\frac{d\delta T_{ld}}{dt} = -\frac{h_{ld}A_d\rho_{ld}}{C_P M_{ld}} * \frac{d\delta L}{dt} + \frac{W_{fw}}{M_{ld}} * \delta T_{fw} + \frac{h_{fw}}{C_P M_{ld}} * \delta W_{fw} - \frac{W_{dc}T_{dc}}{M_{ld}} - \frac{h_{dc}}{C_P M_{ld}} * \delta W_{dc} + \frac{(1-X_e)W_{rm}\frac{\partial h_f}{\partial P_B}}{C_P M_{ld}} * \delta P_B + \frac{(1-X_e)h_f}{C_P M_{ld}} * \delta W_{rm} - \frac{W_{rm}h_f}{C_P M_{ld}} * \delta X_e \quad (4.1)$$

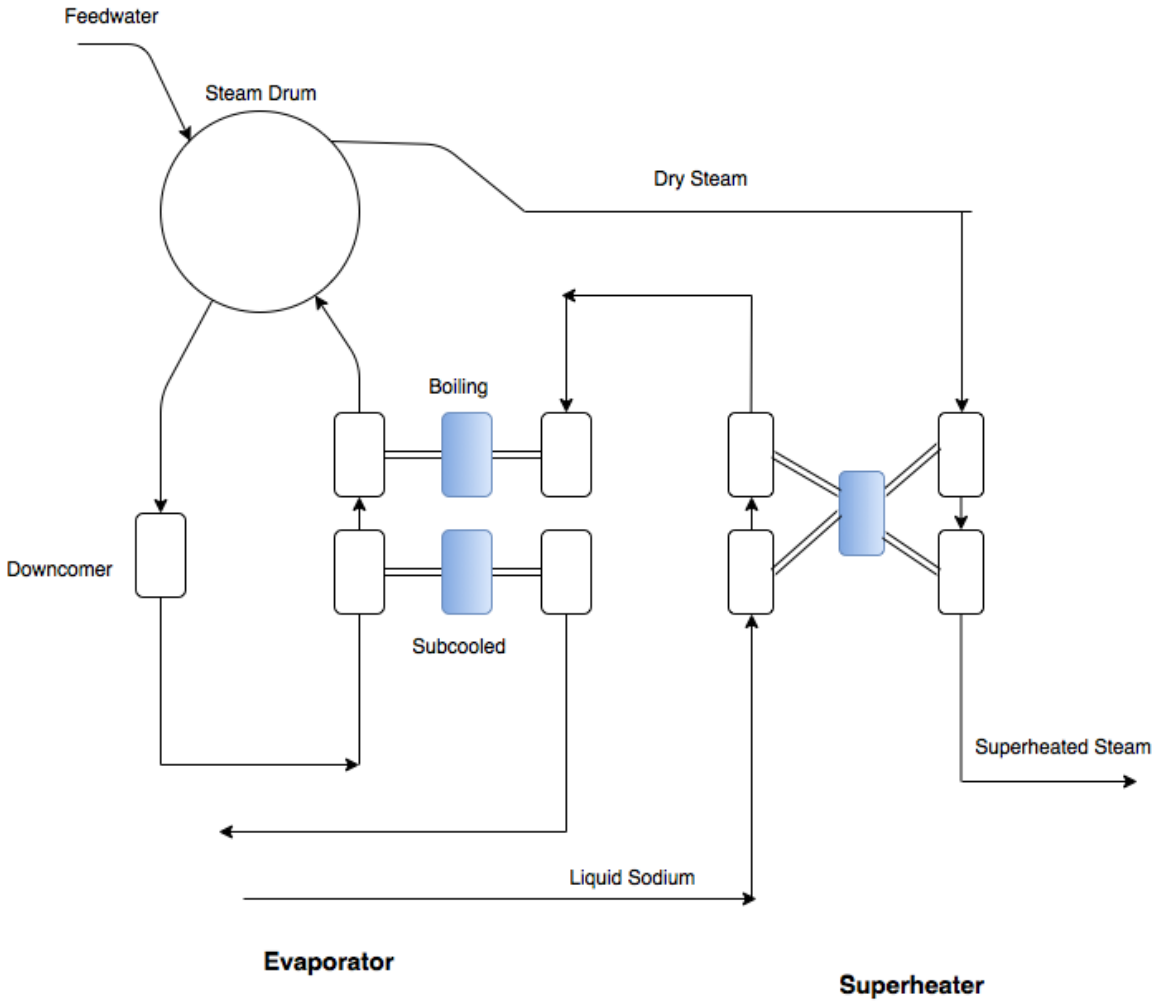


Figure 3.4 Nodal representation of EBR-II steam generator

$$\frac{d\delta P_D}{dt} = \frac{X_e}{V_{SD}\frac{\partial \rho_{ST}}{\partial P_D}} * \delta W_{rm} + \frac{W_{rm}}{V_{SD}\frac{\partial \rho_{ST}}{\partial P_D}} * \delta X_e + \frac{C_L}{V_{SD}\frac{\partial \rho_{ST}}{\partial P_D}} * \delta P_D + \frac{P_D}{V_{SD}\frac{\partial \rho_{ST}}{\partial P_D}} * \delta C_L \quad (4.2)$$

where:
T_{ld} = temperature of liquid in the drum
T_{dc} = downcomer temperature
T_{fw} = feedwater temperature
h_{ld} = enthalpy of liquid in the drum
M_{ld} = mass of liquid in the drum
W_{fw} = feedwater mass flow rate
h_{fw} = enthalpy of the feedwater
L = level in the drum
ρ_{ld} = density of liquid in the drum
A_d = longitudinal area of the drum
W_{dc} = downcomer flow rate
h_f = saturation enthalpy of water
h_{dc} = downcomer water enthalpy
V_{SD} = volume of steam drum
P_D = pressure inside steam drum
ρ_{ST} = density of steam
C_L = steam valve coefficient
W_{rm} = rising water/steam mixture flow rate
X_e = steam exit quality

b Boiling Region

The equations for boiling regions are shown below

$$\frac{d\delta X_e}{dt} = -\frac{A_B\rho_B Z_B\left(\frac{\partial h_f}{\partial P_B}+X_e\frac{h_{fg}}{\partial P_B}\right)+h_B A_B Z_B K_1}{A_B\rho Z_B\frac{h_{fg}}{2}-h_B A_B Z_B K_2} * \frac{d\delta P_B}{dt} + \frac{h_B\rho_B}{\rho Z_B\frac{h_{fg}}{2}-h_B Z_B K_2} * \frac{d\delta Z_{SC}}{dt} +$$
$$\frac{U_{MS1}A_{MS1}}{A_B\rho Z_B\frac{h_{fg}}{2}-h_B A_B Z_B K_2} * \delta T_{M1} + \frac{W_2\frac{\partial h_f}{\partial P_B}-U_{MS1}A_{MS1}\frac{\partial T_{sat}}{\partial P_B}-W_{RM}X_e\frac{\partial h_{fg}}{\partial P_B}+WB3\ h_f}{A_B\rho Z_B\frac{h_{fg}}{2}-h_B A_B Z_B K_2} * \delta P_B -$$
$$\frac{U_{MS1}L_{MS}(T_{M1}-T_{sat})-h_f WB4}{A_B\rho Z_B\frac{h_{fg}}{2}-h_B A_B Z_B K_2} * \delta Z_{SC} - \frac{h_{Xe}}{A_B\rho Z_B\frac{h_{fg}}{2}-h_B A_B Z_B K_2} * \delta W_{rm} - \frac{W_{rm}h_{fg}}{A_B\rho Z_B\frac{h_{fg}}{2}-h_B A_B Z_B K_2} *$$
$$\delta X_e + \frac{h_f WB1}{A_B\rho Z_B\frac{h_{fg}}{2}-h_B A_B Z_B K_2} * \delta T_{MZ} + \frac{h_f WB2}{A_B\rho Z_B\frac{h_{fg}}{2}-h_B A_B Z_B K_2} * \delta T_{DC}$$
(4.3)

$$h_B = h_f\left(1-\frac{X_e}{2}\right) \quad (4.4)$$

$$\rho_B = \rho_f\left(1-\frac{X_e}{2}\right) + \rho_g\frac{X_e}{2} \quad (4.5)$$

$$h_{Xe} = h_f + X_e h_{fg} \tag{4.6}$$

$$\frac{d\delta P_B}{dt} = -\frac{\partial P_B}{\partial T_{sat}} * \frac{d\delta T_{DC}}{dt} - \frac{\partial P_B}{\partial T_{sat}} \frac{T_{DC}+T_{sat}}{Z_{SC}} * \frac{d\delta Z_{SC}}{dt} + \frac{2}{A_{SC}\rho_{SC}Z_{SC}C_{PW}} \frac{\partial P_B}{\partial T_{sat}} (U_{MS1}L_{MS}Z_{SC} - C_{PW}T_{sat}WB1) * \delta T_{M2} - \frac{2}{A_{SC}\rho_{SC}Z_{SC}C_{PW}} \frac{\partial P_B}{\partial T_{sat}} (U_{MS1}L_{MS}Z_{SC} - W_{DC}C_{PW} + C_{PW}T_{sat}WB2) * \delta T_{DC} - \frac{2}{A_{SC}\rho_{SC}Z_{SC}C_{PW}} \left(U_{MS1}A_{MS1} + W_2C_{PW} + C_{PW}T_{sat}WB3 \frac{\partial P_B}{\partial T_{sat}}\right) \delta P + \frac{2}{A_{SC}\rho_{SC}Z_{SC}C_{PW}} \frac{\partial P_B}{\partial T_{sat}} \left[U_{MS1}L_{MS} \frac{2T_{M1}-T_{DC}-T_{sat}}{2} - C_{PW}T_{sat}WB4\right] * \delta Z_{SC} + C_{PW}T_{DC} * \delta W_{DC} \tag{4.7}$$

where:
X_e = steam exit quality
A_B = cross-sectional area of boiling region
Q_{MS1} = heat transfer rate between metal node 1 and boiling region
L_{MS} = unit heat transfer length between metal and secondary nodes
h_{fg} = latent heat of evaporation
Z_B = height of boiling region
h_f = enthalpy of fluid
WB1, WB2, WB3, WB4 = coefficients of approximated flow equation
K_1, K_2 = coefficients given in reference [6]
C_{PW} = specific heat capacity of subcooled water
M_{SC} = mass of subcooled water
W_{DC} = downcomer mass flow rate
W_2 = mass flow rate of water leaving subcooled region
ρ_{SC} = density of subcooled water

c Primary Coolant and Tube Wall Nodes

The equations for primary coolant and tube wall nodes are shown below.

$$\frac{d\delta Z_{SC}}{dt} = \frac{1}{\rho_{SC}A_{SC}} * (W_{PE} - W_{P1}) \tag{4.8}$$

$$\frac{d\delta T_{P1}}{dt} = \frac{1}{\tau_{P1}} * \delta T_{PE} - \left(\frac{1}{\tau_{P1}} + \frac{U_{PM}A_{PM1}}{M_{P1}C_P}\right) * \delta T_{P1} + \frac{U_{PM}A_{PM1}}{M_{P1}C_P} * \delta T_{M1} + \frac{U_{PM}L_{PM}}{M_{P1}C_P} (T_{P1} - T_{M1}) * \delta Z_{SC}$$

$$\frac{d\delta T_{P2}}{dt} + \frac{T_{P1}-T_{P2}}{Z_{SC}} * \frac{d\delta Z_{SC}}{dt} = \frac{1}{\tau_{P2}} * \delta T_{P1} - \left(\frac{1}{\tau_{P2}} + \frac{U_{PM}A_{PM2}}{M_{P2}C_P}\right) * \delta T_{P2} + \frac{U_{PM}A_{PM2}}{M_{P2}C_P} * \delta T_{M2} - \frac{U_{PM}L_{PM}}{M_{P2}C_P} (T_{P2} - T_{M2}) * \delta Z_{SC} \tag{4.9}$$

$$\frac{d\delta T_{M1}}{dt} - \frac{T_{M1}-T_{M2}}{2Z_{SC}} * \frac{d\delta Z_{SC}}{dt} = \frac{U_{PM}A_{PM1}}{M_{M1}C_M} * \delta T_{P1} - \frac{U_{PM}A_{PM}+U_{MS1}A_{MS1}}{M_{M1}C_M} * \delta T_{M1} + \frac{U_{MS1}A_{MS1}}{M_{M1}C_M} \frac{\partial T_{sat}}{\partial P_B} * \delta P_B \tag{4.10}$$

$$\frac{d\delta T_{M2}}{dt} - \frac{T_{M1}-T_{M2}}{2Z_{SC}} * \frac{d\delta Z_{SC}}{dt} = \frac{U_{PM}A_{PM2}}{M_{M2}C_M} * \delta T_{P2} - \frac{U_{PM}A_{PM2}+U_{MS2}A_{MS2}}{M_{M2}C_M} * \delta T_{M2} + \frac{U_{MS2}A_{MS2}}{2M_{M2}C_M}\frac{\partial T_{sat}}{\partial P_B} * \delta P_B + \frac{U_{MS2}A_{MS2}}{2M_{M2}C_M} * \delta T_{DC} \quad (4.11)$$

where:
Z_{SC} = Subcooled height
W_{PE} = mass flow rate at the entrance of the lump
W_{P1} = mass flow rate at the exit of the lump
ρ_P = density of primary sodium
A_P = flow area of primary sodium
T_{Pi} = Bulk mean temperature of primary coolant node i
T_{PE} = Entrance sodium temperature
U_{PM} = Overall heat transfer coefficient between primary and metal lumps
A_{PMi} = Heat transfer area between the metal and primary node i ($A_{PM1} = A_{PM2}$)
M_{Pi} = Mass of sodium in primary coolant node i
τ_{Pi} = residence time of sodium in primary coolant node i
L_{PM} = Unit heat transfer length between primary and metal nodes
T_{Mi} = average metal temperature in metal node i
U_{MSi} = heat transfer coefficient between metal and secondary node i
A_{MSi} = heat transfer area between metal and secondary node i
M_{Mi} = mass of tube metal in node i
T_{DC} = downcomer outlet temperature

d Downcomer

The equations for downcomer are shown as below.

$$\frac{d\delta W_{dc}}{dt} = \frac{g_c A_{dc}}{Z_{dc}} * \delta P_B - \frac{g_c A_{dc}}{Z_{dc}} * \delta P_d - \frac{f_{dc} W_{dc}}{D_{dc} A_{dc} \rho_{dc}} * \delta W_{dc} \quad (4.12)$$

$$\frac{d\delta T_{dc}}{dt} = \frac{1}{\tau_{dc}} * (\delta T_{ld} - \delta T_{dc}) \quad (4.13)$$

where:
A_{dc} = cross sectional area of downcomer pipes
Z_{dc} = height of downcomer pipes
W_{dc} = mass flow rate in downcomer
ρ_{dc} = desnity of downcomer fluid
f_{dc} = friction factor in downcomer piping
D_{dc} = hydraulic diameter
g_c = gravitational constant
P_D = pressure inside steam drum
τ_{dc} = resident time in downcomer piping

e Water/Steam Mixture

The equations for water/steam mixture are shown as below.

$$\frac{d\delta W_{rm}}{dt} = C_1 * \delta P_d + C_2 * \delta P_B + C_3 * \delta Z_{SC} + C_4 * \delta W_{rm} \quad (4.14)$$

$$C_1 = -\frac{g_c A_t}{Z_{ev}} \quad (4.15)$$

$$C_2 = \frac{g_c A_t}{Z_{ev}} - \frac{g_c A_t}{Z_{ev}}\left[Z_{sc}\left(\frac{\partial \rho_{sc}}{\partial P_B}\right) + Z_b\left(\frac{\partial \rho_b}{\partial P_B}\right)\right] + \frac{A_t \phi^2 fo}{2X_{ev} D_t}\left[\frac{f_{sc} Z_{sc}}{\rho_{sc}^2}\left(\frac{\partial \rho_{sc}}{\partial P_B}\right) + \frac{f_b Z_b}{\rho_f^2}\left(\frac{\partial \rho_f}{\partial P_B}\right)\right] \quad (4.16)$$

$$C_3 = (\rho_b - \rho_{sc})\frac{g_c A_t}{Z_{ev}} + \frac{A_t \phi^2 fo}{2 Z_{ev} D_t}\left[\frac{f_b}{\rho_f} - \frac{f_{SC}}{\rho_{SC}}\right] \quad (4.17)$$

$$C_4 = -\frac{f_{sc} Z_{sc} W_{rm}}{A_t Z_{ev} D_t \rho_{SC}} - \frac{f_b Z_b W_{rm}}{A_t Z_{ev} D_t \rho_f}\phi^2 \quad (4.18)$$

where:
W_{rm} = rising water/steam mixture flow rate
Z_b = boiling height
Z_{ev} = height of the evaporator
A_t = cross sectional area of duplex tubes
f_{sc} = friction factor through subcooled region
f_b = friction factor through boiling region
D_t = total hydraulic diameter
ϕ = integral two-phase friction multiplier, defined in (Berkan and Upadhyaya 1988)
ρ_{SC} = density of subcooled region
ρ_b = density of boiling region
X_{ev} = quality of steam in the evaporator
Z_{sc} = height of the subcooled region

3.2.2 Superheater State Equations

*The superhe*ater model considers a single-phase heat transfer regime. Dry steam is heated by the primary sodium to 875 ^{o}F at full power [6]. The superheater is modeled as a five-node counterflow single-phase heat exchanger, using the same equations as the IHX in the primary system model, equatinos (3.19-3.23)

3.2.3 Control Design

The steam generator model responses to four different step perturbations: feedwater temperature; feedwater flow; steam valve opening; inlet sodium temperature.

These four perturbations are the forcing terms of the state-space model. The main control of the steam generator is performed by means of the steam drum level control. The controller accepts four analog signals: steam-drum level, feedwater flow, steam flow

and blowdown flow. The actuator is the feedwater valve. Mathematically, this perturbation was implemented on the corresponding pressure drop. So a PID controller is applied to control the steam pressure.

3.3 The Development of Balance of Plant

The balance of plant (BOP) has a reduced size to accommodate smaller power levels of the reactor, but otherwise contains a general infrastructure and layout. BOP systems have been resized according to the model in [13]. The BOP has been structured to generate an output of feedwater temperature when provided the main steam flow, temperature, and pressure from the steam generator model. The feedwater flow rate is the main user input for manual control of the reactor system. A portion of steam is routed from the steam header to the reheaters, and the remainder is channeled to the nozzle chest as shown in Figure 3.5; this component regulates steam delivery to the high pressure turbine. An inline series of four turbines are connected to a single shaft, which is coupled to the generator. Moisture separator and reheater are between the high and low pressure turbines. Their function is to increase the enthalpy of steam from the high pressure turbine outlet so that it may pass through the low pressure turbines without inducing cavitation of the blades. The low pressure turbine outlets are condensed into feedwater via the heat sink, then reheated and pumped back to the steam generator. The equations for the BOP are given in [13].

The BOP model in [13] was designed for a 180 MWe SMR and had to be sized appropriately for 40 MWe output. The values of three inputs: the flow rate, temperature, and pressure of the superheated steam, were adjusted from the original input to meet the desired BOP conditions. In the PAR model, feedwater flow should be maintained at 75 gpm in order to assure the output power as 40MWe at 100% power level. The parameter adjustment began with a trial to verify the necessity of adjusting the parameters by confirming that the BOP model would not meet the design specifications. The BOP model was isolated from the PAR model and stimulated with the appropriate values from the steam head for the three inputs related to the superheated steam. To achieve the desired value of feedwater flowrate, the distribution of feedwater in the feedwater heaters and moisture separater must be adjusted. Additionally, the look-up tables in the BOP model were expanded to adapt the expected inputs for the smaller plant. The adjustment of feedwater distribution and expansion of look-up tables were iteratively updated through trial and error until the desired feedwater flowrate was achieved.

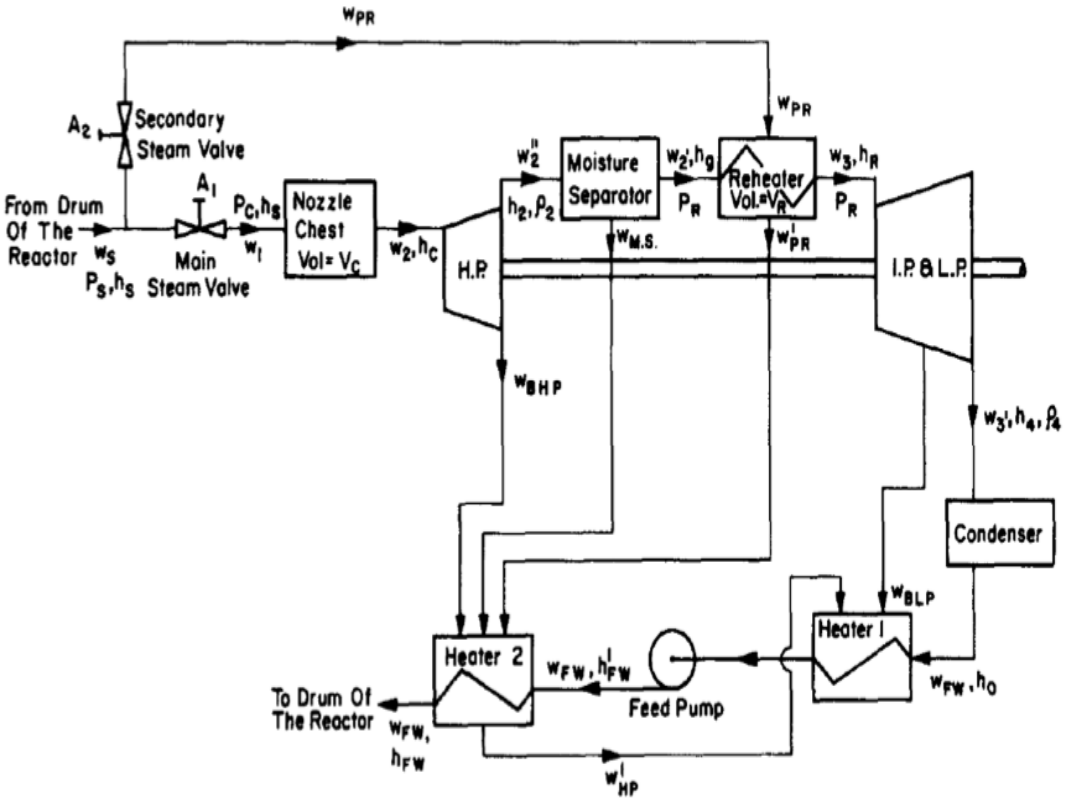


Figure 3.5 Balance of Plant Flow Diagram [12]

Chapter 4

Control Strategy and Model Validation

It is important to develop a subsystem comprised of steam header and feedback system to evaluate and quantify the performance of the two reactor units operating simultaneously, which is connected to a single turbine, resulting in a steam-mixing control problem with respect to unbalanced loads across the two units.

4.1 Steam Header

The superheated steam from the two-steam generator flows into a common header, as shown in Figure 4.1

Steam coming from both units is superheated and any pressure loss between the steam generator exit and the pressure header is neglected. Additional assumptions, specifically concerning the calculation of the temperature of the mixed steam [5], include:

- Steam pressure coming out of the HCSGs remains constant at 1245 psig for the entire range of reactor operation.
- Feed water temperature is fixed at 412°F, corresponding to 100% power for entire simulations.
- Steam mixture temperature at the steam header is calculated assuming constant steam pressure, balance of mass and steam properties, and is calculated as:

$$h_T(t) = \frac{h_1(t)\dot{m}_1 + h_2(t)\dot{m}_2}{\dot{m}_T} \tag{6.1}$$

$$\dot{m}_T = \dot{m}_1 + \dot{m}_2 \tag{6.2}$$

Where:
$h_T(t)$： the temperature-dependent total enthalpy
$h_1(t)$: module 1 temperature-dependent enthalpy
$h_2(t)$: module 2 temperature-dependent enthalpy
$\dot{m}_T$, $\dot{m}_1$, $\dot{m}_2$: total, module1 and module 2 steam mass flow rates

The values of $h_T(t)$ obtained from the combined steam temperatures are then used to determine the temperature of the mixed steam at the corresponding superheated steam pressure of 1245 psig using a look-up table; this assumes that steam outlet pressure deviations can be neglected.

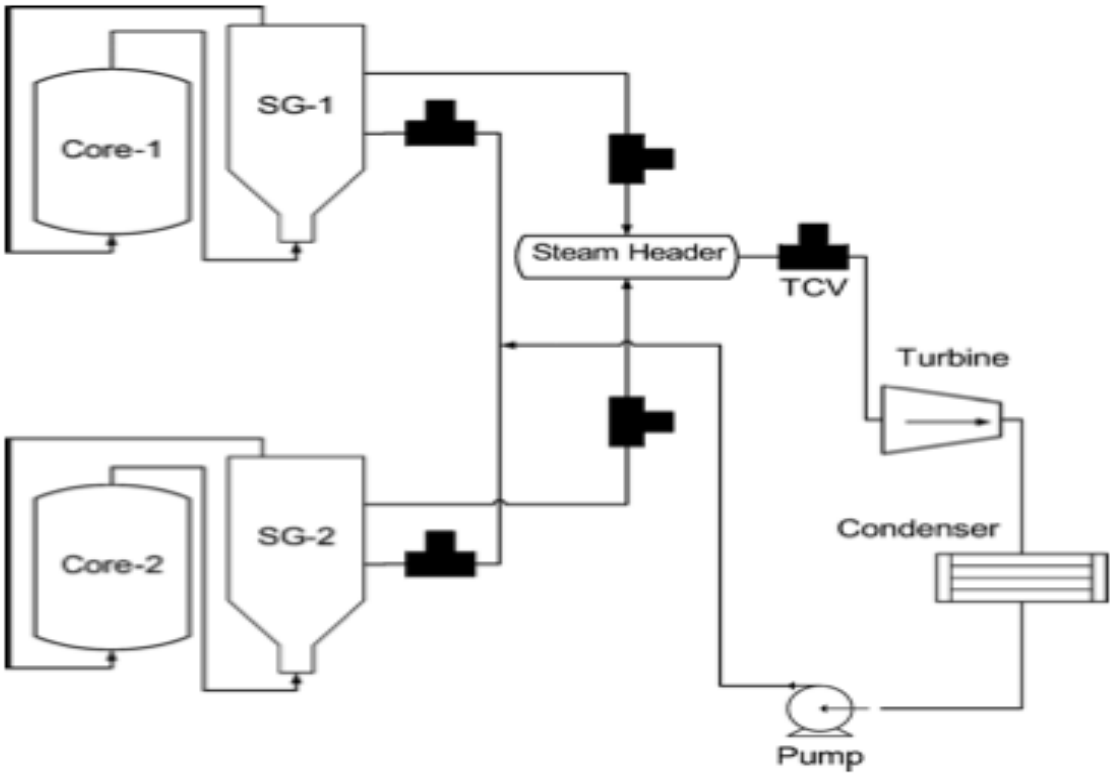


Figure 4.1 Schematic diagram of a multi-modular power block [5]

4.2 Feedback Between Units

In a two-modular nuclear power plant, it is expected that each unit will have its own feed water controller, and any primary system feedback between units will be very limited, since the reason all units can operate at different power rates for most of their individual fuel cycles to allow only one of the units to be out for refueling at a time.

To simulate a stronger dependency between both modules, other than that at the steam header, module 2 has its feed water flow allowed to change based on the ratio of both instant power demands multiplied by the nominal power-dependent feed water flow of module 1[5].

$$\dot{f}_2 = \frac{P_2(t)}{P_1(t)} \dot{f}_1(P_1) \tag{6.3}$$

Where:
$\dot{f}_1, \dot{f}_2$: module 1 and 2 feed water flows
$P_1(t), P_2(t)$: module 1 and 2 time-dependent power demands

4.3 Daily Load Profile

Load following is the capability of a reactor to follow changes in the grid demand; for example, the load may changes during the day 24h as shown in Figure 4.2. And the maximum output is 40MWe. Hence, it is desirable from an economical point of view that a two-modular reactor plant be able to do the same, although there are currently no regulations in this regard. For this purpose, the two-module model with steam mixing is subjected to transients similar to Figure 4.2. And degradation of primary and intermediate sodium pumps could limit ability to meet power demand

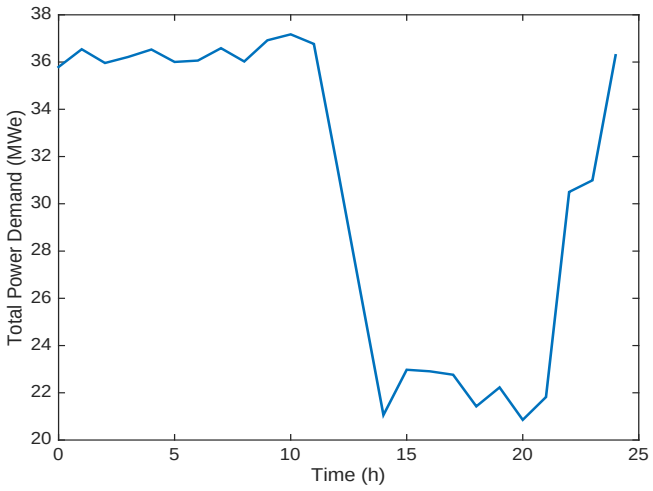


Figure 4.2 Power level for daily load profile

4.4 Steam Generator Control Design

Four different step perturbations are the forcing terms of the state-space model. The main control of the steam generator is performed by means of the steam drum level control. The controller accepts four analog signals: steam-drum level, feedwater flow, steam flow, and blowdown flow. The actuator is the feedwater valve. A PID controller is applied to control the steam pressure by assuming a linear relationship between the valve opening and the corresponding pressure drop. Figure 4.3 and 4.4 shows the plot of superheated steam temperature and drum pressure responding with the -5 cents reactivity perturbation. The temperature of superheated temperature decreases around -15 F with the degraded power, and -6.5 psi for the drum pressure.

4.5 Model Validation

The response of the primary system model was compared to the perturbation model response reported in [6] for both fractional core power and sodium tank temperature following a -5 cent reactivity insertion. Figure 4.5 shows the reactor fractional power response to a -5 cent reactivity perturbation in the PAR model and the EBR-II model.

The sodium tank temperature response of the PAR and EBR-II models is also shown in Figure 4.6. In both figures, the EBR-II model response is the perturbation from steady state conditions at 100% powe. For the step reactivity perturbation of -5 cents, it indicates that the temperature response of the tank sodium settles down at about 2500s. This delayed temperature deviation will affect the core and reflector regions as the recycling sodium temperature reaches the tank temperature. The effect of the tank sodium temperature on the core power can be seen in Figure 4.5. The time response of the primary system model is observed to be in three modes: the prompt jump (0 to 1s), the reactivity feedback settlement (1 to 200s), and delayed thermohydraulic effects (200 to 3000s). The results of the nonlinear PAR model match with the results of the original EBR-II perturbation model for this reactivity insertion.

Figure 4.7 shows reactor fractional power response to different step reactivity insertions: -5, -10, and -15 cents. The model response follows expected behavior for these insertions, though no results were available for the EBR-II model for comparison for the larger reactivity insertions.

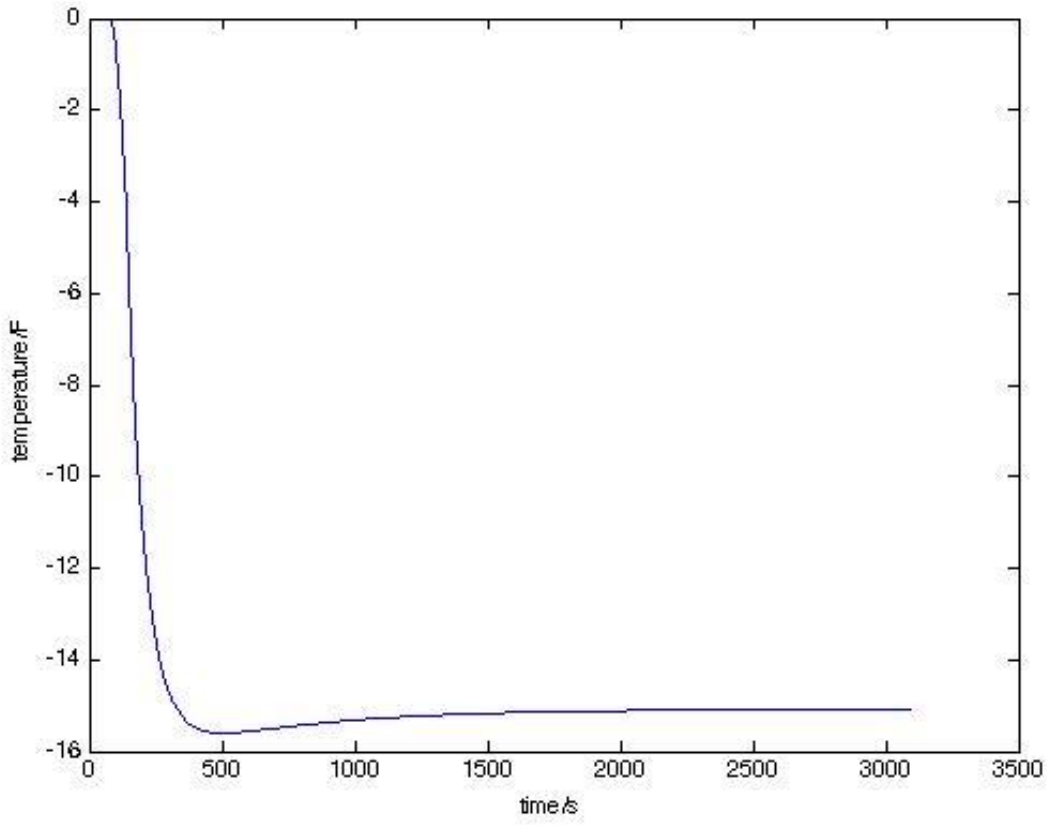


Figure 4.3 Perturbation model response of superheated steam temperature to a -5 cents reactivity perturbation

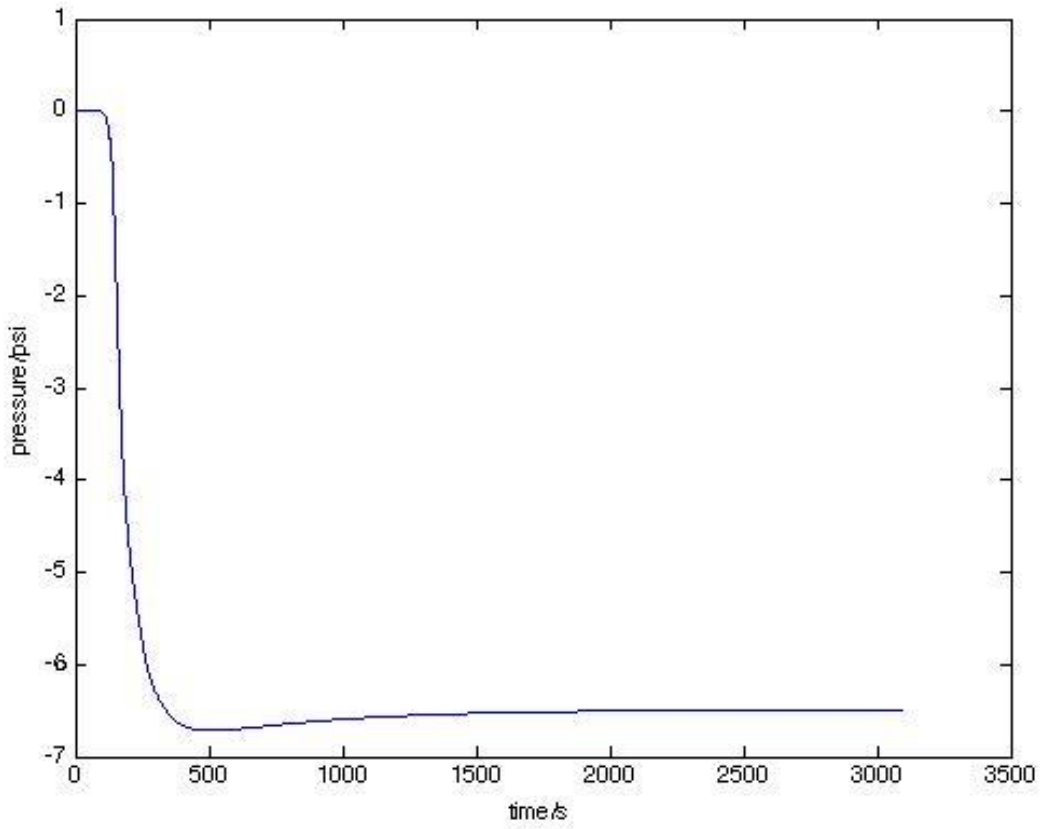


Figure 4.4 Perturbation model response of drum pressure to a -5 cents reactivity perturbation

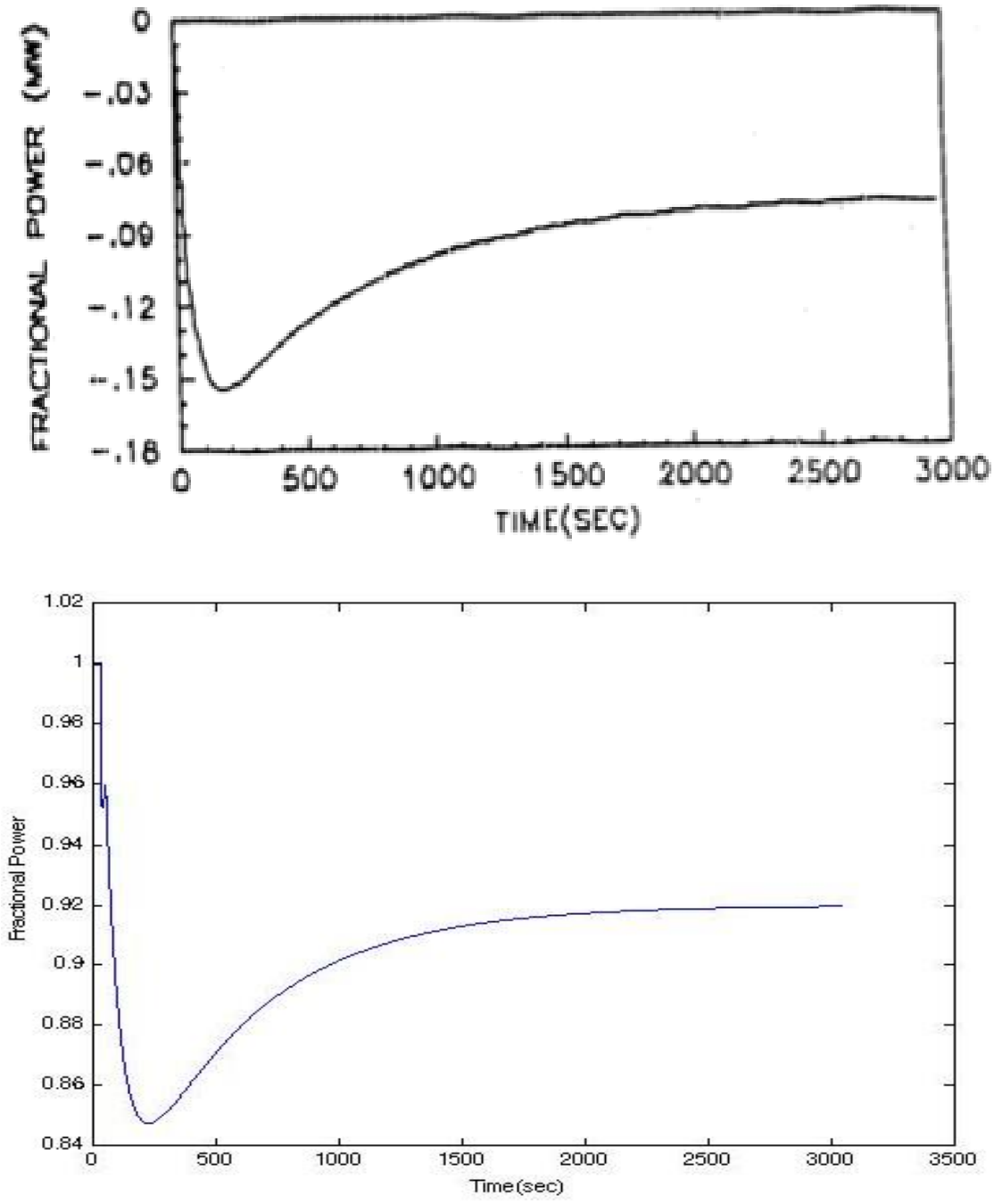


Figure 4.5 Step response of fractional reactor power to a -5 cents reactivity perturbation in (lower) PAR model and (upper) EBR-II model [6]

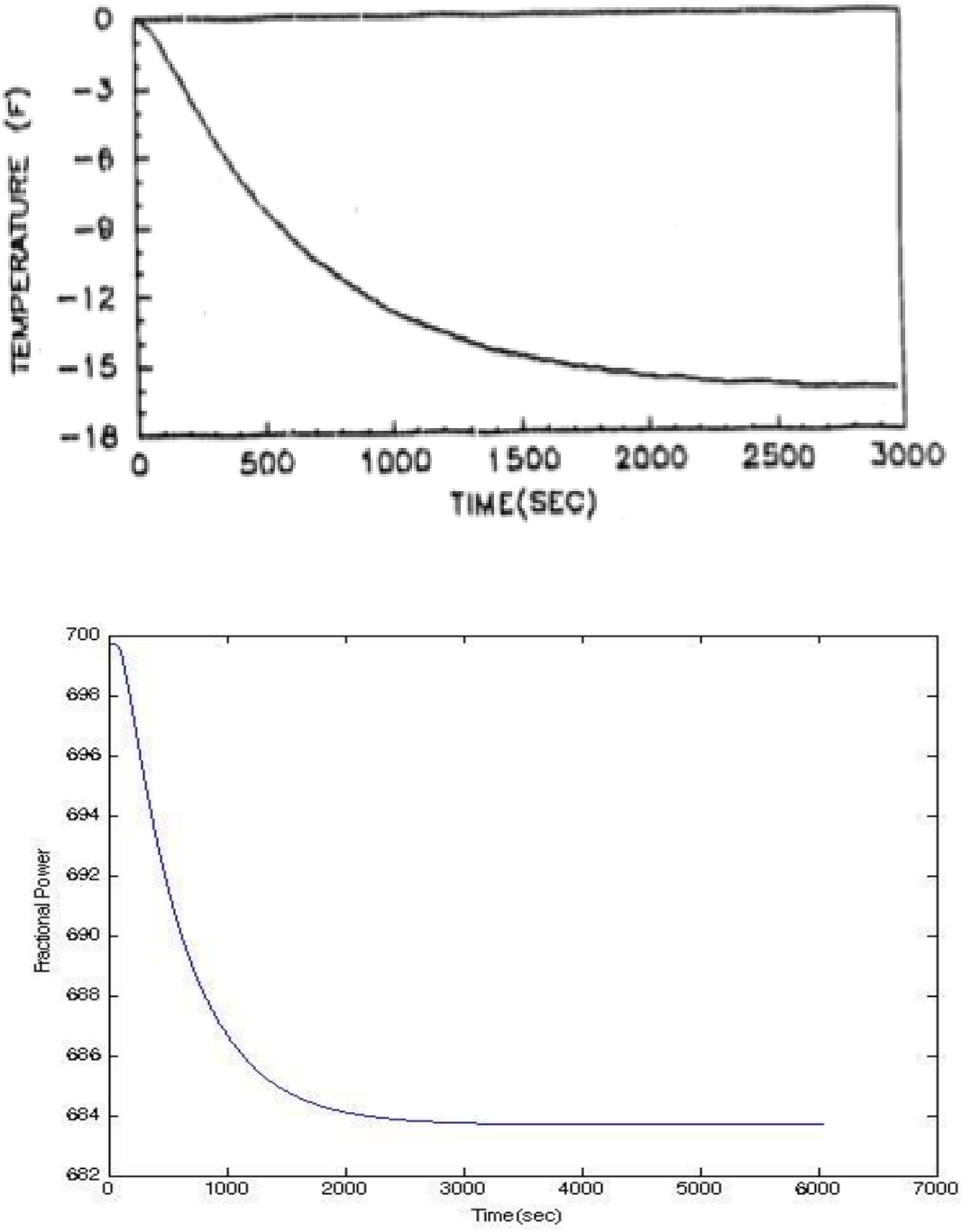


Figure 4.6 Step response of sodium tank temperature to -5 cents reactivity perturbation in (lower) PAR model and (upper) EBR-II model [6]

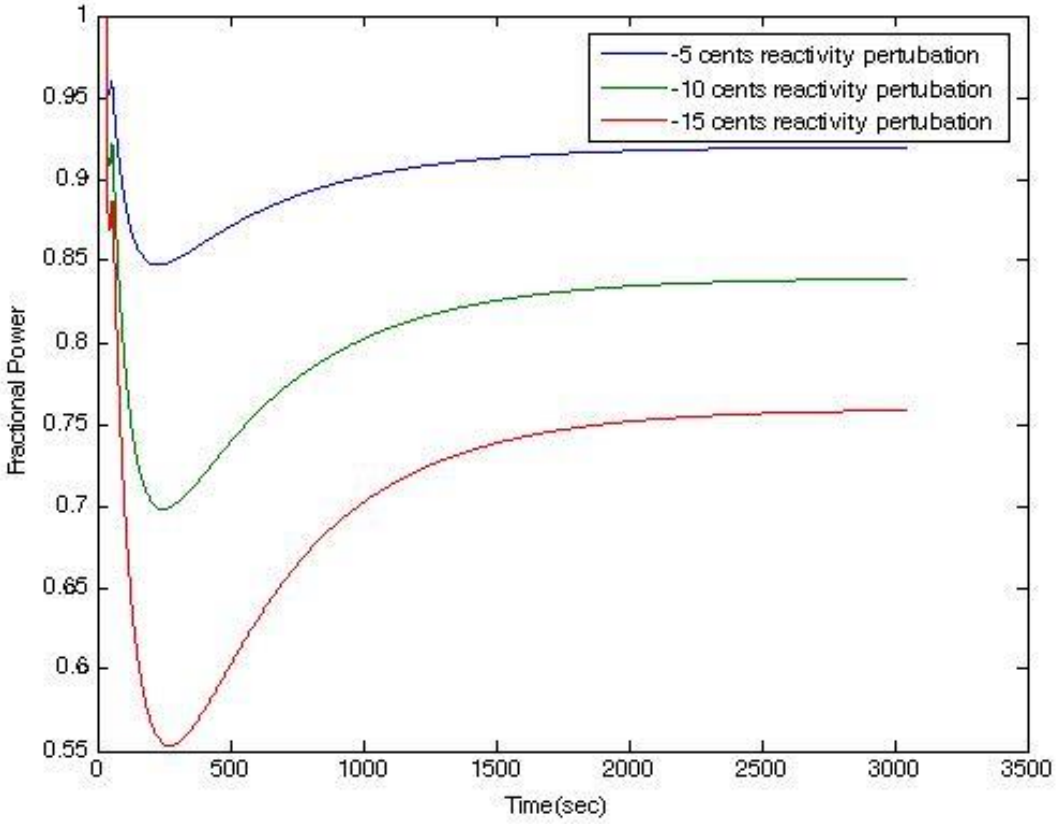


Figure 4.7 Step response of fractional reactor power to different reactivity perturbation

Chapter 5

Pump Degradation Modeling and Response

5.1 Pump Degradation Modeling

Modeling the degradation of electromagnetic sodium pumps is difficult; no literature has been found to date that reports on the failure characteristics of these pumps. Centrifugal pump degradation due to cavitation can be modeled according to well-known pump curves [10]; models of degradation of mechanical pumps are employed for the purposes of demonstrating the ERM. This follows previous work in modeling pump degradation in an integral pressurized water reactor [17]. The degraded pump curves due to pump cavitation are shown in Figure 5.1, where the pump curve is regenerated for each degradation level by making the following transform of the flow rate:

$$Q_p^* = \frac{Q}{p} \tag{7.3}$$

where p is the fraction of flow rate remaining, i.e. for the first degraded condition, where 99% of the flow is still available, p = 0.99. This effectively shifts the pump curves in along the flow variable, adjusting for the lost flow rate. By changing the flow rate in each loop, we can simulate pump degradation.

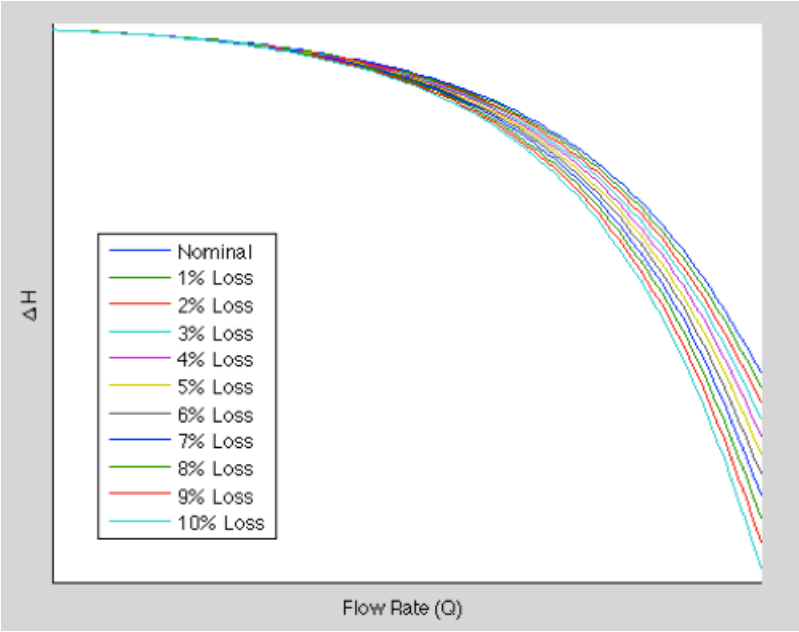


Figure 5.1 Degraded pump curves [10]

5.2 Pump Degradation Response

Figure 5.2 and 5.3 show that in the condition of coolant pump degradation, the core power corresponds with different flow rate. The model results show that the degradation of primary or secondary sodium pumps leads to the decreasing core power.

Due to negative temperature feedback effects, as the primary coolant temperature increases, fractional core power will decrease. The loss of flow in either primary or intermediate sodium loops, due to pump degradation, will lead to an increase in coolant temperature and a corresponding decrease in core power. In the extreme case of zero flow in either case, the reactor will shut down, as shown in Figure 5.4. In the case of complete loss of primary flow, the core power decreases to zero after ~100 seconds with no other action (e.g., control rod drop). Loss of secondary flow leads to core shut down in ~2200 seconds. However, degradation of the primary and intermediate sodium pumps, not complete failure, is of greater interest to the current research.

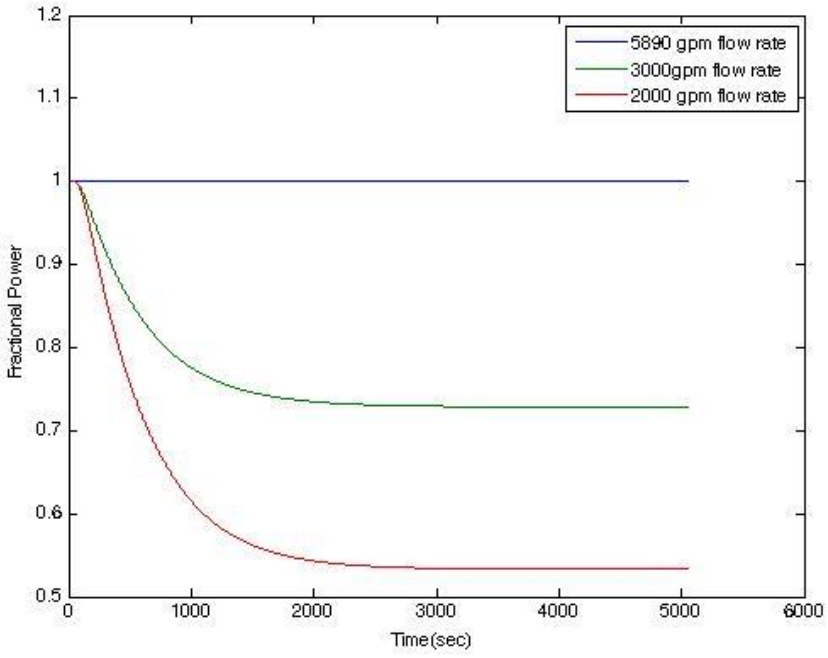


Figure 5.2 Fractional power with different secondary side flow rate

Table 5.1 gives the steady state fractional power for reduced flow conditions in the primary or intermediate sodium. The results indicate that the core power decreases as pump degradation leads to reduced flow in either primary or intermediate loops. The component condition and performance has a direct impact on overall plant performance.

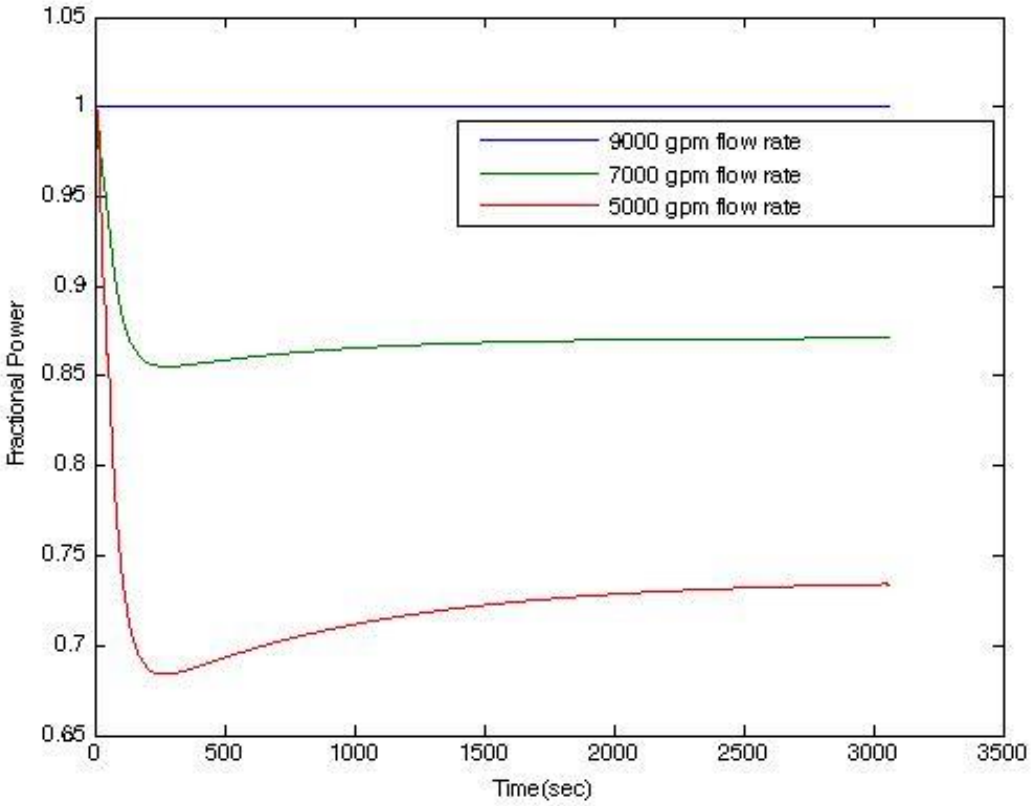


Figure 5.3 Fractional power with different primary side flow rate

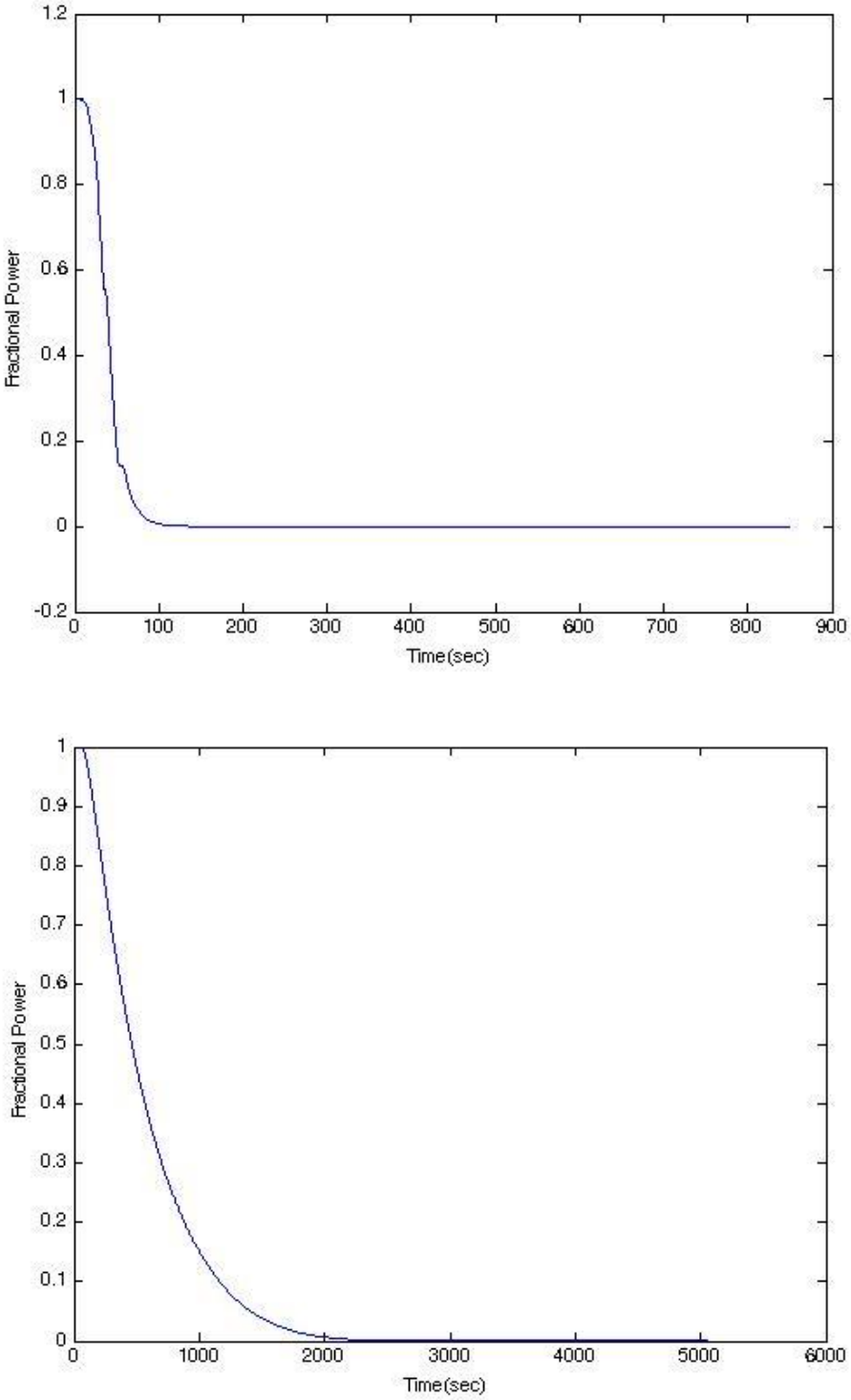


Figure 5.4 Core Fractional Power response to complete loss of flow in (upper) primary and (lower) secondary sodium

Table 5.1 Steady state fractional core power with degraded primary or intermediate flow conditions

Primary Sodium Flow Rate (gpm)	Intermediate Sodium Flow Rate (gpm)	Fractional Core Power
9000	5890	1.0
7000	5890	0.87
5000	5890	0.74
9000	3000	0.74
9000	2000	0.53

For an individual module with degradation of a single pump. The steady state fractional core power as a function of flow rate is shown for intermediate and primary sodium pumps in Figures 5.5 and 5.6, respectively. As the plots shown, the fractional power increases with the increase of either intermediate or primary sodium flow rate until it reaches full power.

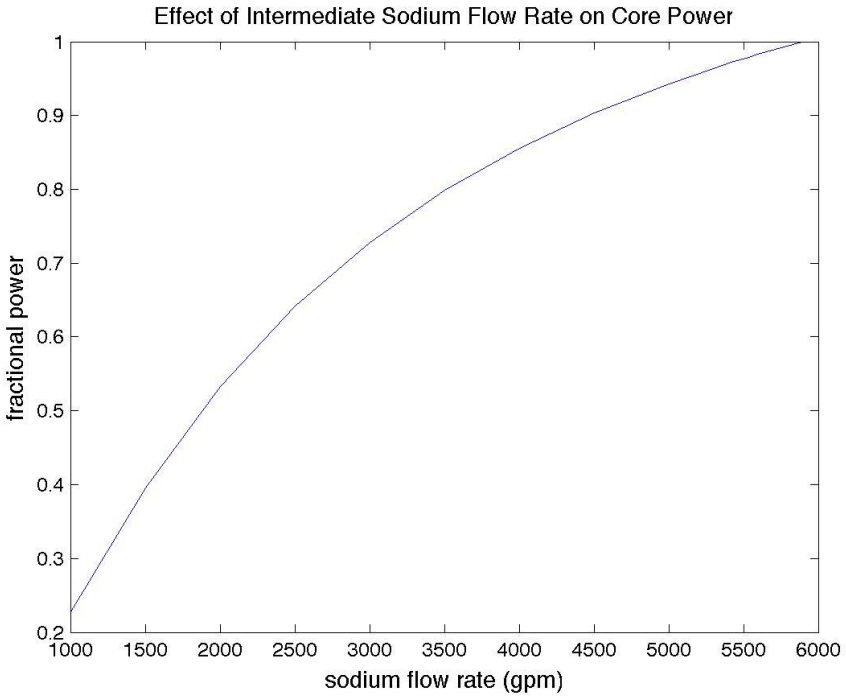


Figure 5.5 Step response of fractional power with the degraded intermediate sodium flow rate

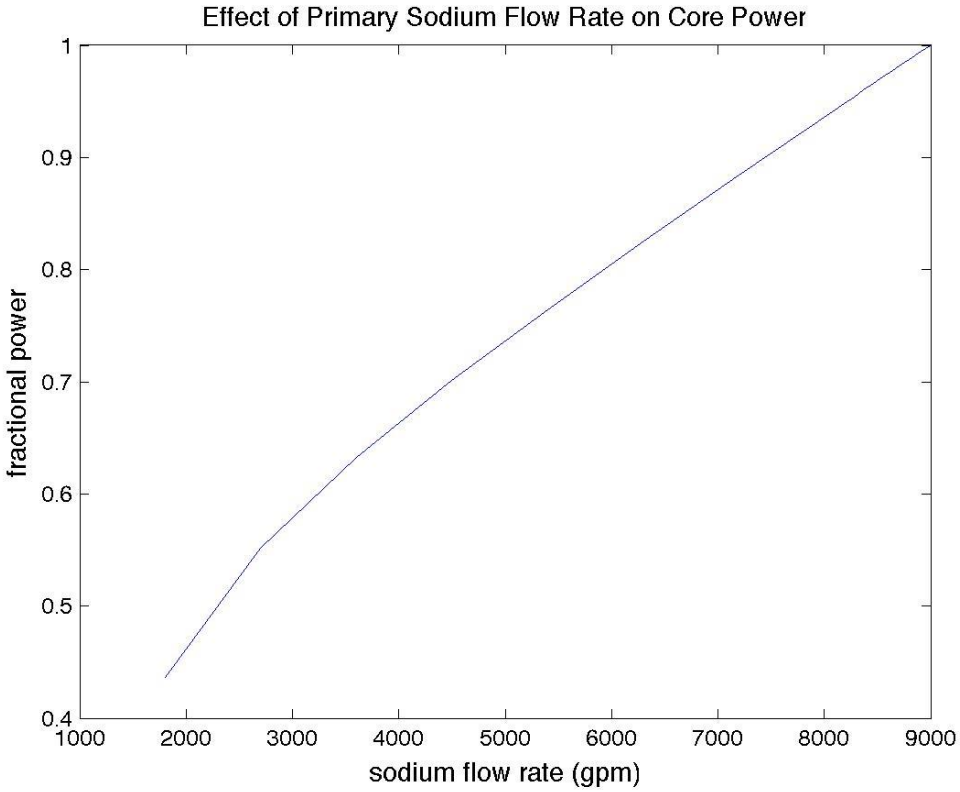


Figure 5.6 Step response of fractional power with the degraded primary sodium flow rate

Reduced flow rate limits maximum power output from a module as can be seen from Figure 5.7. As flow decreases, negative reactivity feedback reduces the total power output. And output from two modules can compensate for small reductions in power output while still meeting the full demand profile

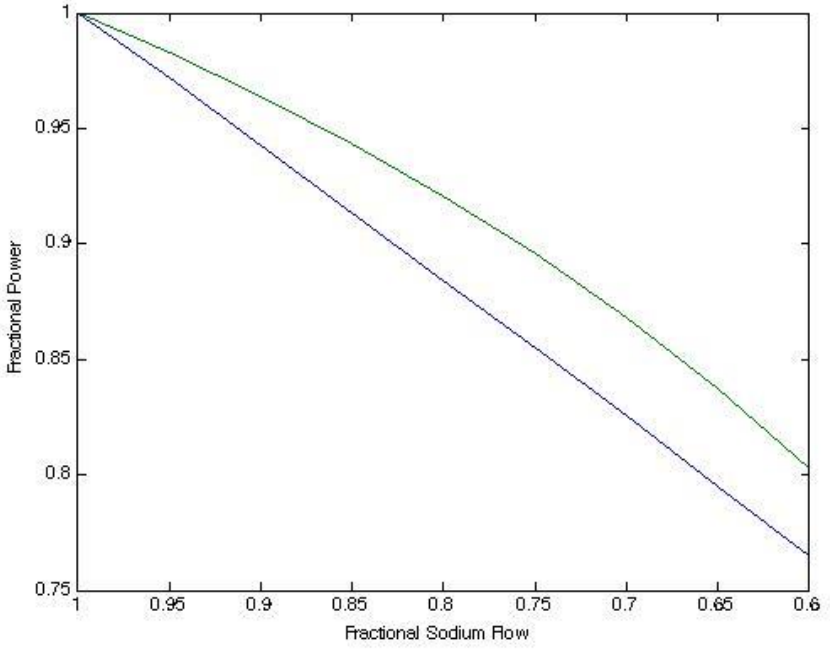


Figure 5.7 Fractional power with degraded primary or intermediate sodium pump

For the implementation of fuzzy control, Figure 5.8 and 5.9 shows that the module 2 remains at around 80% percent of its power at the largest flow rate, while the power of module 1 is 100%. So the total power is around 36.83 if there is no pump degradation.

The fractional power of module 2 reaches 100% when the primary sodium flow rate of module 1 decreases to 6700 gpm. Meanwhile, the fractional power of module 1 is around 80% power rate. And the total power stays 100% at this point. This is the function of fuzzy control that makes the total power at 100% power level even though the flow rate keeps decreasing. Considering the case that the fractional power of module 2 cannot be larger than 100%, and the fractional power of module 1 keeps decreasing, the total power will decrease corresponding with the dropping power of module 1. This applies to the decreasing intermediate sodium flow rate as well. The total power can be remained at 100% from 5890 gpm to around 4234 gpm.

The daily and night demand for the plant is around 37 MWe and 22 MWe according to Figure 5.9. For the degradation of primary pump, the total power can be remained at 100% from 9000gpm to 6700 gpm. So a negative external reactivity by rod insertion can be added to reaches the demand. As the flow rate keeps dropping down, the daily demand cannot be met even if no external reactivity is added, then the even low demand at night as well.

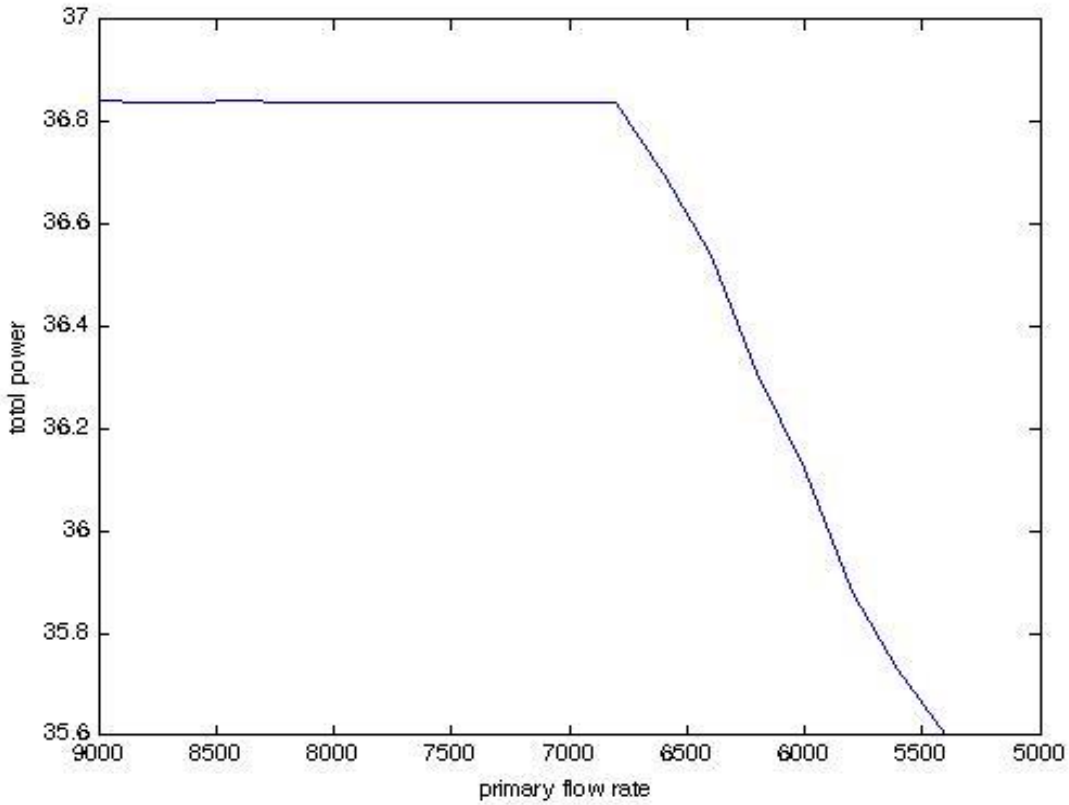


Figure 5.8 Total power output with the primary pump degradation in module 1

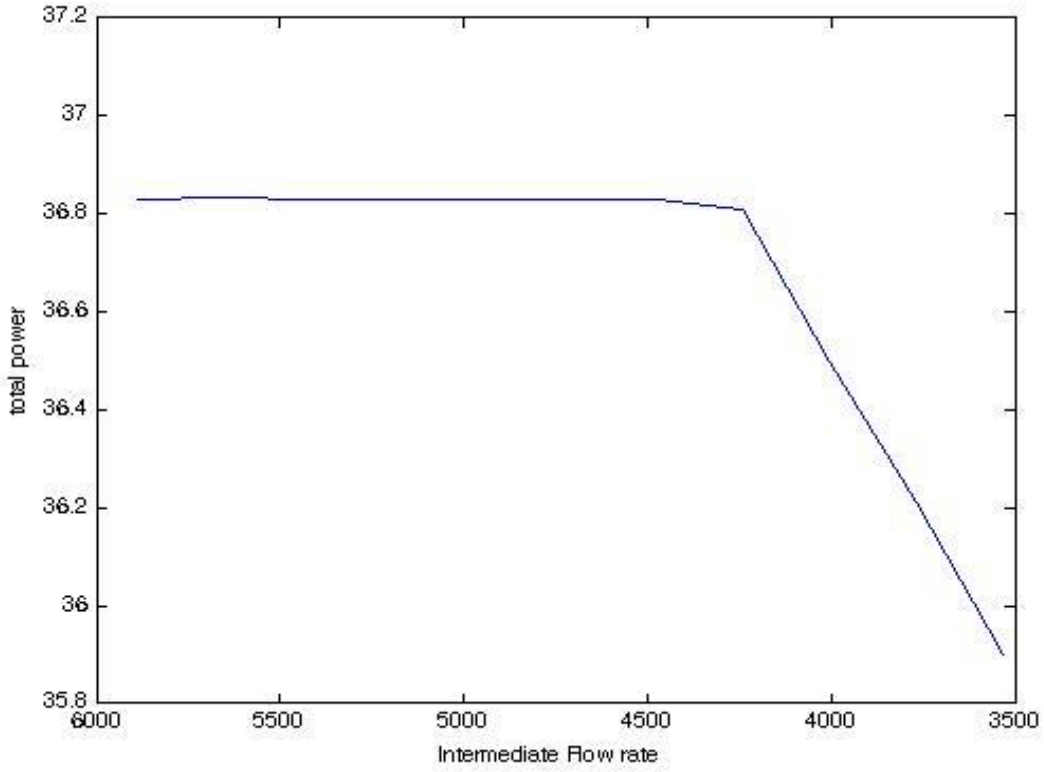


Figure 5.9 Total power output with the intermediate pump degradation in module 2

Chapter 6

Summary and Future Work

The enhanced risk monitor (ERM) has been proposed to address limitations in the available operational experience and failure data for advanced reactor designs. Current risk monitors evaluate the point-in-time risk of a plant operating under its specific configuration, but it does not consider the current and evolving condition of key components and systems. The ERM incorporates equipment condition assessment and prognostic results for key active components to provide a more accurate characterization of system risk.

This report presents on the dynamic simulation of the nonlinear model of a multi-modular prototypical advanced reactor developed to demonstrate the efficacy of the proposed ERM. Degradation of primary and intermediate pumps was numerically simulated, and the effect on core fractional power was simulated. As sodium flow rate decreased due to pump degradation, power output decreased. The total power can be remained at 100% from 9000gpm to 6700 gpm for the primary pump degradation of module 1, and 5890 gpm to 4230 gpm for the intermediate pump degradation. So the daily load may not be met if the total power is not remained at 100% with lower flow rate, either the 6700 gpm or 4230 gpm.

The described effort provides initial data to evaluate the ERM framework for advanced reactors. The developed model adequately simulates the full reactor power block under normal operation. However, in order to fully evaluate the ERM, additional degradation modes should be added beyond the current pump degradation capability. In addition, measurements that can be related to component performance (either direct measurements of performance or indicators inferred from process parameters) should be added in order to develop appropriate equipment condition assessment and prognostic models to provide the probability of failure information that the ERM requires to evaluate the operational risk.

The current fuzzy controller can be easily replaced with more advanced controllers or a risk-informed controller. Additional manipulated variables can also easily be added by augmenting the reactor equations. For instance, the primary and intermediate sodium flow rates can be used as manipulated variables to control key temperatures and power levels; currently, these flow rates are only related to the flow capacity of the appropriate pump.

List of References

[1] Coble, J.B., et al., Technical Needs for Enhancing Risk Monitors with Equipment Condition Assessment for Advanced Small Modular Reactors, PNNL-22377, SMR/ICHMI/PNNL/TR-2013/02. 2013, Pacific Northwest National Laboratory (PNNL), Richland, WA (US).
[2] H. Bailly, D. Ménessier, C. Prunier. The Nuclear Fuel of Pressurized Water Reactors and Fast Neutron Reactors Lavoisier (1999)
[3] J. A, Bernard, A. F. Henry, D. D. Lanning, and J. E. Meyer, Studies on the closed-loop digital control of multi-modular reactors, Rep. MITNRL-049, Mass. Inst. Technol., Cambridge, MA, Nov. 1992.
[4] K. K. Kim, Design and simulation of a digital control system for a multi-modular power plant, Ph.D. dissertation, Dep. Nucl. Eng., Mass. Inst. Technol., Cambridge, MA, Aug. 1992.
[5] S. R. Perillo and B.R. Upadhyaya, Control and Instrumentation Strategies for Multi-Modular Integral Nuclear Reactor Systems. IEEE Transactions on Nuclear Science, Vol58, No.5, 2011.
[6] Berkan, R.C. and B.R. Upadhyaya, Dynamic Modeling of EBR-II for Simulation and Control. 1988, University of Tennessee: Knoxville, TN.
[7] Sackett, J., Operating and Test Experience for the Experimental Breeder Reactor II (EBR-II), in Global 2009. 2009: Paris, France.
[8] W Chang, L., et al., Demonstration of EBR-II power maneuvers without control rod movement. Nuclear Engineering and Design, 1989. 113(1): p. 141-148
[9] Ramuhalli, P., et al., Technical Report on Preliminary Methodology for Enhancing Risk Monitors with Integrated Equipment Condition Assessment. 2013: Pacific Northwest National Laboratory
[10] Grist, E., Cavitation and the centrifugal pump: a guide for pump users. 1998: CRC Press.
[11] J. D. Malloy. Control system and method for pwr systems. United States Patent Application Publication, US 2012/0155594 A1, 2012
[12] A. T. Chen. A digital simulation for nuclear once through steam generators. Department of Nuclear Engineering , The university of Tennessee, 1976.
[13] J. R. Kapernick. Dynamic Modeling of a Small Modular Reactor for control and Monitoring. University of Tennessee: Knoxville, TN.
[14] P.V. Shankar. Simulation model of a nuclear reactor turbine. Nuclear Engineering and Design, 44:269–277, 1977.
[15] A. Dutta and I. Thangamani. Simulation model of nuclear power plant-turbine. Bhabha Atomic Research Centre, 2006.
[16] B.R. Upadhyaya and M. Naghedolfeizi. Dynamic modeling of a pressurized water reactor plant for diagnostics and control. Department of Nuclear Engineering, The University of Tennessee, DE-FG07-88ER12824, 1991.
[17] Hines, J. W., B. R. Upadhyaya and J. B. Coble (2011). Advanced Instrumentation and Control Methods for Small and Medium Reactors with IRIS Demonstration. Knoxville, Tennessee, The University of Tennessee.
[18] OECD Nuclear Agency for the Generation IV International Forum, 2014

Vita

Xiaotong Liu was born in Shijiazhuang, China in 1992. He grew up in Beijing where he attended High School affiliated to Peking University

In 2014, he received a B.S degree in science from Harbin Engineering University. And he decided to continue his study to pursue a Master degree in nuclear engineering. His professional work experience and interests include risk and system analysis, fault detection, diagnostics and prognostics.